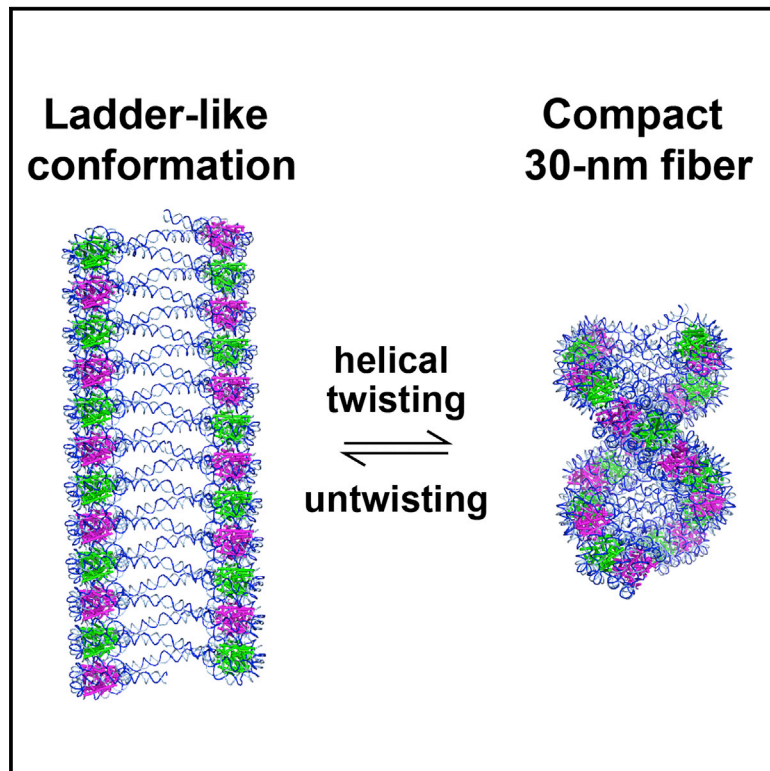# Structure of an H1-Bound 6-Nucleosome Array Reveals an Untwisted Two-Start Chromatin Fiber Conformation

Graphical Abstract

Highlights

- Crystal structure of a 6-nucleosome array was determined in complex with histone H1

- The array adopts a ladder-like conformation half as compact as a twisted 30-nm fiber

- Cryo-EM, biophysical, and biochemical experiments confirm the ladder-like structure

- A shift in ionic conditions induces the array to switch to a compact twisted state

Authors

Isabel Garcia-Saez, Hervé Menoni, Ramachandran Boopathi, ..., Dimitar Angelov, Carlo Petosa, Stefan Dimitrov

Correspondence

jan.bednar@univ-grenoble-alpes.fr (J.B.), hamiche@igbmc.fr (A.H.), dimitar.anguelov@ens-lyon.fr (D.A.), carlo.petosa@ibs.fr (C.P.), stefan.dimitrov@univ-grenoble-alpes.fr (S.D.)

In Brief

Garcia-Saez et al. report the crystal structure of a 6-nucleosome array bound to histone H1, revealing an untwisted fiber conformation only half as compact as a twisted 30-nm chromatin fiber. Shifting the ionic conditions induces a more compact, twisted fiber structure, providing insights into the conformational plasticity of chromatin.

CellPress

Structure of an H1-Bound 6-Nucleosome Array Reveals an Untwisted Two-Start Chromatin Fiber Conformation

Isabel Garcia-Saez,[1,7] Hervé Menoni,[2,3,7] Ramachandran Boopathi,[2,3,7] Manu S. Shukla,[2,3,7,8] Lama Soueidan,[2,3,7] Marjolaine Noirclerc-Savoye,[1] Aline Le Roy,[1] Dimitrios A. Skoufias,[1] Jan Bednar,[2,5,*] Ali Hamiche,[4,*] Dimitar Angelov,[3,*] Carlo Petosa,[1,*] and Stefan Dimitrov[2,6,9,*]

[1]Université Grenoble Alpes, CNRS, CEA, Institut de Biologie Structurale (IBS), 38000 Grenoble, France
[2]Université Grenoble Alpes, CNRS UMR 5309, INSERM U1209, Institute for Advanced Biosciences (IAB), Site Santé – Allée des Alpes, 38700 La Tronche, France
[3]Université de Lyon, Ecole Normale Supérieure de Lyon, CNRS, Laboratoire de Biologie et de Modélisation de la Cellule LBMC, 46 Allée d'Italie, 69007 Lyon, France
[4]Département de Génomique Fonctionnelle et Cancer, Institut de Génétique et Biologie Moléculaire et Cellulaire (IGBMC), Université de Strasbourg, CNRS, INSERM, 67404 Illkirch Cedex, France
[5]Laboratory of the Biology and Pathology of the Eye, Institute of Biology and Medical Genetics, First Faculty of Medicine, Charles University and General University Hospital in Prague, Albertov 4, 128 00 Prague 2, Czech Republic
[6]"Roumen Tsanev" Institute of Molecular Biology, Bulgarian Academy of Sciences, Sofia, Bulgaria
[7]These authors contributed equally
[8]Present address: Wellcome Centre for Cell Biology and Institute of Cell Biology, School of Biological Sciences, The University of Edinburgh, Swann Building, King's Buildings, Mayfield Road, Edinburgh EH9 3BF, UK
[9]Lead Contact
*Correspondence: jan.bednar@univ-grenoble-alpes.fr (J.B.), hamiche@igbmc.fr (A.H.), dimitar.anguelov@ens-lyon.fr (D.A.), carlo.petosa@ibs.fr (C.P.), stefan.dimitrov@univ-grenoble-alpes.fr (S.D.)
https://doi.org/10.1016/j.molcel.2018.09.027

SUMMARY

Chromatin adopts a diversity of regular and irregular fiber structures *in vitro* and *in vivo*. However, how an array of nucleosomes folds into and switches between different fiber conformations is poorly understood. We report the 9.7 Å resolution crystal structure of a 6-nucleosome array bound to linker histone H1 determined under ionic conditions that favor incomplete chromatin condensation. The structure reveals a flat two-start helix with uniform nucleosomal stacking interfaces and a nucleosome packing density that is only half that of a twisted 30-nm fiber. Hydroxyl radical footprinting indicates that H1 binds the array in an on-dyad configuration resembling that observed for mononucleosomes. Biophysical, cryo-EM, and crosslinking data validate the crystal structure and reveal that a minor change in ionic environment shifts the conformational landscape to a more compact, twisted form. These findings provide insights into the structural plasticity of chromatin and suggest a possible assembly pathway for a 30-nm fiber.

INTRODUCTION

Eukaryotic nuclear DNA is packaged in nucleosomes, which in turn condense into higher-complexity structures. At low ionic strength, purified chromatin forms 11-nm "beads on a string" filaments with an open zigzag conformation (Griffith, 1975; Ris and Kubai, 1970; Thoma et al., 1979; Makarov et al., 1983). Raising the ionic strength leads progressively to a closed zigzag structure, further compaction, and the formation of 30-nm fibers (Greulich et al., 1987; Thoma et al., 1979; Makarov et al., 1983). Under physiological conditions, chromatin extracted from diverse cell types adopts a 30-nm fiber configuration (Thoma et al., 1979; Belmont and Bruce, 1994; Belmont et al., 1987; Bednar et al., 1998), which consequently has been intensely studied as a paradigm of higher-order chromatin structure. *In vivo*, 30-nm fibers are notably absent from many eukaryotic nuclei, where chromatin appears to form irregularly folded chains (Eltsov et al., 2008; Fussner et al., 2012; Gan et al., 2013; Nishino et al., 2012; Ou et al., 2017; Cai et al., 2018) with zigzag features (Hsieh et al., 2015; Grigoryev et al., 2016; Cai et al., 2018). However, the nuclei of certain terminally differentiated cells contain well-defined 30-nm fibers (Langmore and Schutt, 1980; Woodcock, 1994; Kizilyaprak et al., 2010; Scheffer et al., 2011), suggesting a role for such structures in transcriptionally silent chromatin. Indeed, recent data suggest that H3K9me3-marked repressed chromatin regions are associated with compact two-start helical fiber structures (Risca et al., 2017). More generally, the wide variety of chromatin configurations observed *in vitro* and *in vivo* underscores the great structural plasticity of chromatin, whose molecular basis, however, remains only poorly understood.

Whereas atomic details are known for how nucleosomal DNA wraps around the core histone octamer (Luger et al., 1997) and interacts with linker histones (Zhou et al., 2013, 2015; Bednar et al., 2017), how a flexible array of nucleosomes condenses into a more

compact chromatin fiber remains elusive. *In vitro* studies have primarily supported one of two configurations for the 30-nm chromatin fiber: a one-start helix with a consecutive arrangement of nucleosomes (Finch and Klug, 1976; Robinson et al., 2006) and a two-start structure comprising two separate nucleosomal stacks (Worcel et al., 1981; Williams et al., 1986; Dorigo et al., 2004; Schalch et al., 2005; Song et al., 2014; Ekundayo et al., 2017). Data have also been reported supporting a heteromorphic combination of one- and two-start structures within the same fiber (Grigoryev et al., 2009) as well as a polymorphic fiber model that incorporates variability in nucleosome repeat length (Collepardo-Guevara and Schlick, 2014). Taken together, the above studies suggest that nucleosomal arrays adopt a diversity of configurations depending on the precise biochemical context.

Studies of H1-bound chromatin extracted from cell nuclei revealed that the salt-dependent compaction and electro-optical properties of nucleosome arrays undergo a sharp transition when the number of nucleosomes increases from 5 to 6 (Marion and Roux, 1978; Butler and Thomas, 1980), suggesting that the minimal unit recapitulating key features of an extended chromatin fiber *in vitro* is a hexanucleosome. In living cells, nucleosomes have been found to cluster in discrete domains, termed "clutches," along the chromatin fiber, with a mean clutch size ranging from 4 to 8 nucleosomes, depending on the cell type (Ricci et al., 2015). Thus, the study of short chromatin fragments such as a 6-nucleosome array may provide useful insights into the fundamental properties of chromatin.

In this study, we report the crystal structure of a hexanucleosome bound to linker histone H1 together with *in vitro* studies of H1-bound 6-, 12-, and 24-nucleosome arrays. Our crystal structure reveals a two-start configuration in which nucleosomes stack through uniform interfaces and adopt a flat zigzag organization whose packing density is half of that reported for twisted 30-nm fibers. We confirm the uniform stacking and two-start organization using a procedure that couples disulfide crosslinking with qPCR, and we verify the flat and extended array conformation in biophysical experiments. High-resolution footprinting data indicate that the globular H1 domain localizes to the dyad axes of the 6-nucleosome array, resembling the binding mode observed for H1- and GH5-bound mononucleosomes (GH5 is the globular domain of H5; Zhou et al., 2015; Bednar et al., 2017) but distinct from that observed for a condensed 12-nucleosome array (Song et al., 2014). Using cryoelectron microscopy (cryo-EM), we identify ionic conditions in which the flat array co-exists with a twisted conformation characteristic of a compact 30-nm fiber and show that a small increase in Mg^{2+} concentration preferentially stabilizes the twisted state. Taken together, our results confirm a two-start organization for short nucleosome arrays *in vitro* and suggest a possible pathway by which these condense into a 30-nm fiber. Furthermore, our findings provide insights into how chromatin may switch between different conformations in response to small changes in local environment.

RESULTS

The Hexanucleosome Forms a Flat Two-Start Helix

We determined the crystal structure of a 6-nucleosome array in stoichiometric complex with full-length H1 (Figure 1A). The array

was reconstituted from recombinant human core histones, *Xenopus laevis* linker histone H1.0b, and six tandem repeats of a 187-bp DNA duplex comprising the 601 positioning sequence (Lowary and Widom, 1998) plus 40 bp of linker DNA. Diffraction data were collected at 9.7 Å resolution (Table 1), and the structure was solved by molecular replacement using the nucleosome core particle (NCP) as a search model. The resulting map revealed strong linker DNA density for the core-proximal DNA helical turn and weaker density for the distal turn, yielding sufficiently clear connectivity between nucleosomes to allow reliable tracing of the DNA path (Figure 1B; Video S1). In contrast, the density for histone H1 was too weak to allow interpretation, presumably reflecting the two-fold disorder that results from the ability of H1 to adopt two dyad-related orientations on each nucleosome (Bednar et al., 2017).

The hexanucleosome forms a two-start helix in which consecutive nucleosomes are related by pseudo-2-fold screw symmetry about the fiber axis (Figures 1C, 1D, and S1), giving rise to a remarkably flat structure whose depth is roughly the diameter of a single nucleosome. The structure deviates from perfect helical symmetry in that the dyad axes of the central nucleosomes (N3 and N4) are orthogonal to the fiber axis, whereas those of the peripheral nucleosomes are tilted by 20°–30° (Figure S1; angle α). These tilted nucleosome orientations yield favorable stacking interactions between neighboring arrays in the crystal and are presumably induced or stabilized by crystallization (Figure S2). The DNA linkers exhibit a pronounced bend midway along their length, comprising two angles: a uniform (~45°) bend in the plane perpendicular to the fiber axis (Figures S3A and S3B, angle φ) and a variable (−35° to +28°) bend in the orthogonal plane (Figure S3C, angle ψ) that compensates for the tilted orientations of the peripheral nucleosomes (Figure S3D) and is absent from the central N3-N4 linker (ψ = 0°). The above deviations from ideal helical geometry suggest a dynamic conformational landscape in solution in which the peripheral nucleosome orientations fluctuate significantly compared with the more highly constrained central nucleosomes. Nevertheless, the fact that the hexanucleosome crystallized indicates that it forms a relatively stable structure, consistent with its ability to recapitulate biophysical properties of longer nucleosome arrays (Marion and Roux, 1978; Butler and Thomas, 1980).

The Array Has Low Nucleosome Packing Density

The degree of nucleosome array condensation strongly depends on the ionic environment (Butler and Thomas, 1980; Korolev et al., 2010; Allahverdi et al., 2015). Our crystals were obtained by hanging drop vapor diffusion in the absence of divalent cations under conditions in which the NaCl concentration gradually increased from 50 to 100 mM during vapor equilibration. In this concentration range and up to 125 mM NaCl, H1-bound hexanucleosomes have been reported to become increasingly compact with increasing ionic strength (Butler and Thomas, 1980), suggesting that the crystal conformation may represent that of an incompletely condensed array. Indeed, consecutive nucleosomes in the crystal structure are separated by a mean helical rise of 28 Å (Figure S1B, distance *h*), corresponding to a packing density of 3.9 nucleosomes per 11 nm. This is markedly lower than previous estimates for condensed chromatin fibers
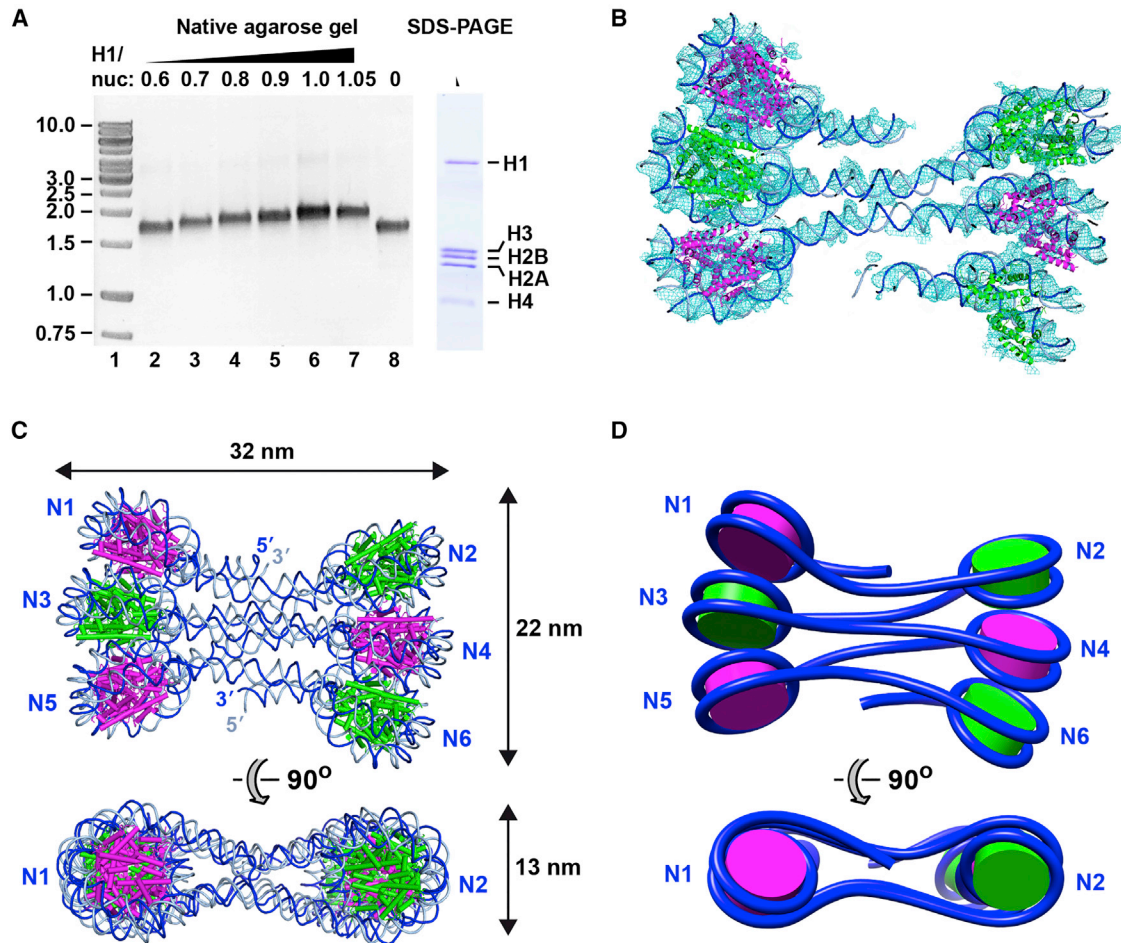
Figure 1. Hexanucleosome Crystal Structure

(A) Sample preparation. Left: native agarose (1.2%) gel showing titration of the hexanucleosome by H1. The best diffracting crystals were obtained at an H1/nucleosome molar ratio of 1.0. Right: denaturing SDS-PAGE (18%) gel of a hexanucleosome prepared with an H1/nucleosome ratio of 1.

(B) Composite $2F_o$-F_c omit map contoured at 1.0 σ.

(C) Crystal structure. Core histones are shown in magenta and green and DNA in dark and light blue.

(D) Cartoon highlighting the connectivity between nucleosomes.

See also Figures S1–S3 and Video S1.

(6.5–12.7 nucleosomes/11 nm) (Gerchman and Ramakrishnan, 1987; Grigoryev et al., 2009; Robinson et al., 2006; Scheffer et al., 2011; Woodcock et al., 1984) and only approximately half that observed in the cryo-EM structure of a condensed 12 × 187 bp nucleosome array (7 nucleosomes/11 nm; Song et al., 2014).

Although the structure by Song et al. (2014) and our hexanucleosome structure (for convenience referred to below as "condensed 12-mer" and "6-mer," respectively) share the same left-handed topology, they exhibit striking conformational differences. These include an ~30° difference in nucleosome orientation relative to the fiber axis and a 12° difference in azimuthal rotation angle relating consecutive nucleosomes (Figure S1B, angles β and θ, respectively). The latter difference equates to a dramatic change in helical periodicity (2 nucleosomes per helical turn for the 6-mer versus ~13 for the condensed 12-mer). This is most easily visualized by extrapolating the heli-

cal geometry of the 6-mer to generate a hypothetical extended array: whereas the two nucleosomal stacks twist around each other in the condensed 12-mer, they adopt a parallel, zigzag configuration in the 6-mer-derived model (Figures 2A and 2B). This lack of twist rationalizes the lower nucleosome packing density of the 6-mer. Notably, the ladder-like appearance of the 6-mer-derived model is highly reminiscent of the "double track" structures observed for chromatin fibers isolated from chicken erythrocytes in 40 mM NaCl (Scheffer et al., 2012) and of a hypothetical fiber model based on the crystal packing of a GH5-bound mononucleosome (Zhou et al., 2018), both characterized by nucleosomes that stack in parallel columns.

Nucleosomes Stack through Uniform Interfaces

The nucleosome stacking arrangement is a distinguishing feature of our 6-mer structure. In the condensed 12-mer, nucleosomes stack through two types of interface: a tight interface

Table 1. Crystallographic Statistics

	PDB: 6HKT
Data Collection[a]	
Synchrotron beamline	ESRF ID23-1
Wavelength (Å)	0.99187
Space group	$P22_12_1$
Unit cell dimensions	a = 111.1 Å, b = 238.8 Å, c = 674.4 Å
Resolution range (Å)	49.1–9.70
(Outer shell)	(10.85–9.70)
Number of measured reflections	72,005 (21,507)
Number of unique reflections	11,252 (3,152)
Multiplicity	6.4 (6.8)
Completeness (%)	99.2 (100)
Mean I/sigma(I)	7.0 (2.3)
R_{merge}	0.211 (0.881)
R_{meas}	0.230 (0.954)
R_{pim}	0.090 (0.362)
$CC_{1/2}$	0.998 (0.604)
Refinement	
Resolution used for refinement	49.1–9.7
Reflections used (total/R_{free})	10,632/572
R_{work}/R_{free}	26.18/29.07
Number of Atoms/Mean B-Factor	
All	82,014/540
Core histones	36,012/451
Core DNA	35,833/574
Linker DNA	9676/736
RMS deviations	0.004
Bond distances (Å)	
Bond angles (°)	0.721
Ramachandran analysis (%)	97.2/0.3
Favored/outliers	
Molprobity analysis	12.67/1.77
Clash Score/overall score	

[a]Values in parentheses are for the highest-resolution shell.

within each tetranucleosome unit and a looser interface between such units, hereafter designated "type I" and "type II," respectively (Figure 2C; Song et al., 2014). Both are included in a recent survey of NCP-NCP interactions (Korolev et al., 2018). By contrast, the stacking interfaces in our 6-mer are highly uniform and of the type II class (Figure 2D). This agrees with the finding that isolated NCPs in 150 mM NaCl preferentially associate through a type II-like interface, whereas few or no type I associations were observed (Bilokapic et al., 2018). In the condensed 12-mer, the type II interface is stabilized by interactions between basic H4 tail residues and the H2A-H2B acidic patch on the adjacent nucleosome (Song et al., 2014). Similar interactions presumably also occur in the 6-mer (Figure S4A). The H2A N-terminal tail is also within contact distance of DNA from the neighboring nucleosome and could conceivably stabilize nucleosomal

stacking, as suggested by a recent computational study (Korolev et al., 2018). Protein-DNA interactions may additionally stabilize the 6-mer type II interface given that several basic residues in H2A and H2B localize close to the core DNA of an adjacent nucleosome (Figure S4A).

Crosslinking Confirms a Two-Start Structure with Uniform Interfaces

To validate our crystal structure, we sought biochemical evidence for a two-start helix with uniform type II interfaces. To this end, we exploited two observations: an H1-bound nucleosome array forms internucleosome disulfide crosslinks when H4 residue Val21 and H2A residue Glu64 are mutated to cysteine (Dorigo et al., 2004); and such crosslinks are compatible with a type II but not a type I interface (Figures S4B and S4C). Based on these observations, we developed a novel assay, termed "identification of closest neighbor nucleosomes" (ICNN), to analyze the interfaces in a nucleosome array. Although this assay was poorly informative when tested on 6-nucleosome arrays (because nucleosomes at the ends of an array yield inefficient crosslinking), it worked well with 12- and 24-nucleosome arrays. The approach is outlined for a 24-nucleosome array in Figures 3 and S5. Each nucleosome in the array contains 147 bp of 601 DNA plus 50 bp of linker DNA. The central 12 nucleosomes (designated N1–N12) contain unique core nucleotides allowing specific amplification by qPCR and a unique restriction site (as well as a common ScaI site) within the linker DNA (Figures 3A, S5A, and S5B). These are flanked on either side by six identical nucleosomes (each with an AvaI site in the linker DNA). Specific cleavage and religation allow targeted biotin labeling of the central repeats. Nucleosomes are reconstituted using H4 and H2A histones containing mutations V21C and E64C, respectively. Following H1 deposition, nucleosomes are crosslinked via the cysteine -SH groups and digested with ScaI and AvaI, yielding mononucleosomes and crosslinked oligonucleosomes (Figure 3B). The crosslinking is performed under ionic conditions (50–80 mM NaCl) similar to those used for crystallization of the 6-mer. Biotinylated particles are then isolated on streptavidin beads in the absence or presence of DTT, which abolishes the crosslinking. The DNA is then purified, and 12 separate qPCR amplification reactions are performed to identify which of the 12 central nucleosomes are tethered to the biotinylated nucleosome through one or more disulfide crosslinks.

We prepared nucleosome arrays using DNA specifically biotinylated on repeat N5, verifying full nucleosome occupancy by restriction analysis (Figure 3C, lanes 3–7) and quantitative histone H1 binding by native gel electrophoresis (Figure 3C, lanes 8–10). Disulfide formation was induced with oxidized glutathione, and the efficiency of internucleosome crosslinking was confirmed by ScaI/AvaI digestion and SDS-PAGE (Figures 3D and 3E). Crosslinked arrays were completely digested with ScaI/AvaI and purified by a streptavidin pull-down, followed by qPCR to identify the eluted nucleosomes. As expected, the strongest signal (defined as 100%) was observed for the biotinylated nucleosome N5 (Figure 4A, right). For unreduced H1-bound arrays, the two next strongest signals were for nucleosomes N3 and N7 (~40%), followed by N1 and N9 (~26%) and finally N11 (17%). No signals were detected for even-numbered
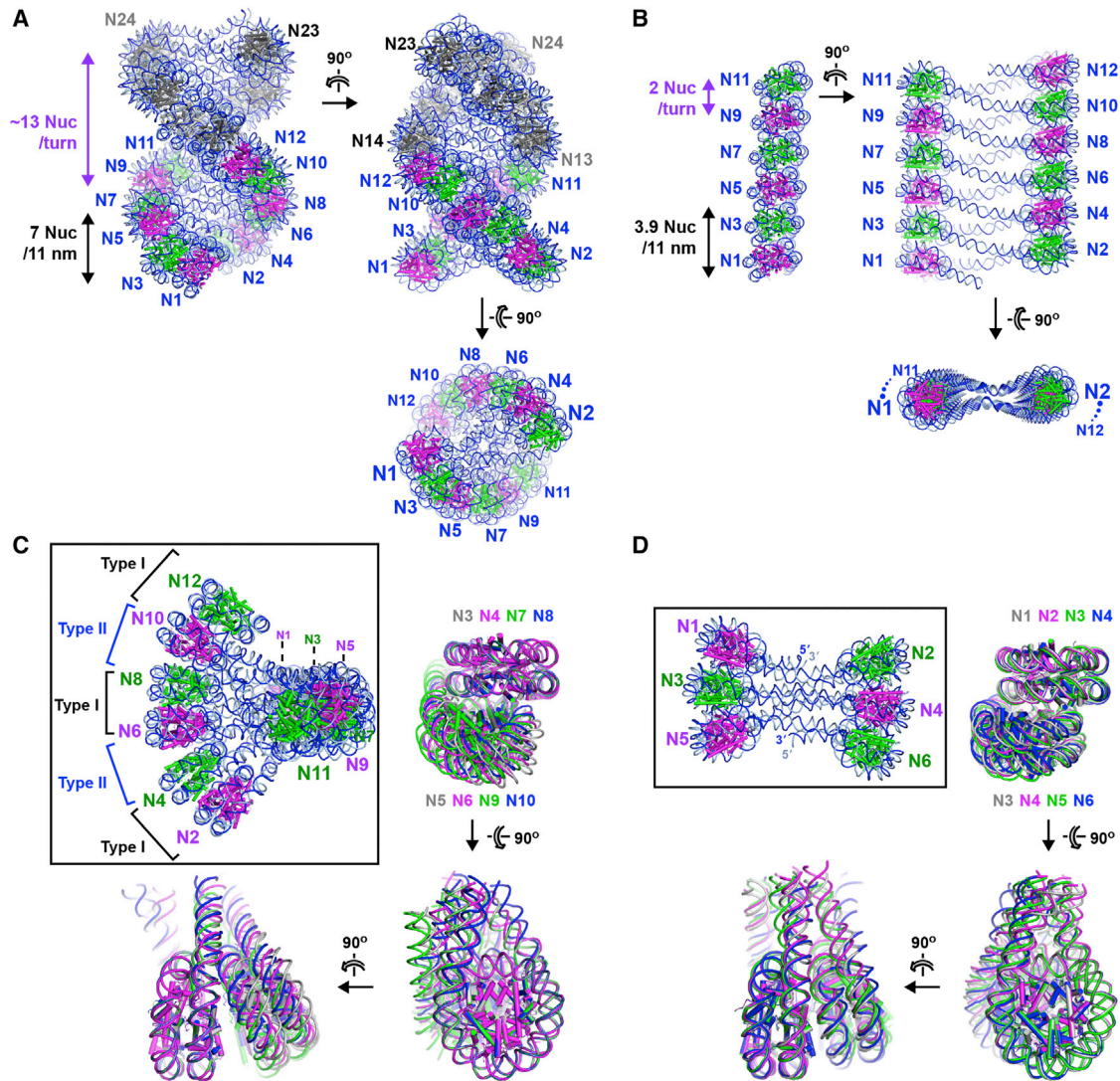
Figure 2. Fiber Conformation and Nucleosome Stacking

(A) Condensed 12-mer (Song et al., 2014). Core histones are shown in green and magenta. The array is extended by 12 nucleosomes (gray) to make evident the twisted helical structure.

(B) Model of an untwisted fiber based on the 6-mer crystal structure, generated from the helical parameters of the N3-N4 dinucleosome.

(C) Inset: condensed 12-mer with type I and II interfaces indicated. Main: alignment of the four dinucleosome units spanning a type II interface. Structures were aligned via the first nucleosome in each pair.

(D) Inset: 6-mer crystal structure. Main: the four dinucleosome stacking units are compared by aligning the first nucleosome of each pair.

nucleosomes. DTT-treated samples or arrays prepared without H1 yielded signals only for N5, confirming that signals for the other odd-numbered nucleosomes are dependent on H1 and on the integrity of the H4-H4 and H2A-H4 disulfide bridges (Figure 4A). The observed signal intensities suggest that N5 forms direct crosslinks with both N3 and N7 and is tethered to N1, N9, and N11 through a "daisy chain" of crosslinked particles comprising at least three (N1-N3-N5 and N5-N7-N9) or four (N5-N7-N9-N11) odd-numbered nucleosomes, respectively. Repeating the analysis with a 24-nucleosome array biotinylated on nucleosome N4 yielded significant signals for N4 (100%) and for N2, N6, N8, N10, and N12 (43%, 39%, 29%, 15%, and 11%,

respectively) but not for odd-numbered nucleosomes (Figure 4A, left). The combined data reveal that, within the H1-bound array, nucleosome N_i forms crosslinks with nucleosomes $N_{i \pm 2}$.

To verify whether the ICNN results depended on DNA linker length, we repeated the assay for 12-nucleosome arrays comprising tandem repeats of 177, 197, or 227 bp, in each case biotinylated on either nucleosome N4, N8, or N9. Comparable results were observed for all three repeat lengths. Strong signals were observed for nucleosomes N2, N6, and N8 from N4-biotinylated arrays; for N4, N6, N10, and N12 from N8-biotinylated arrays; and for N5, N7, and N11 from N9-biotinylated arrays (Figure 4B). In each case, the signal strength decreased
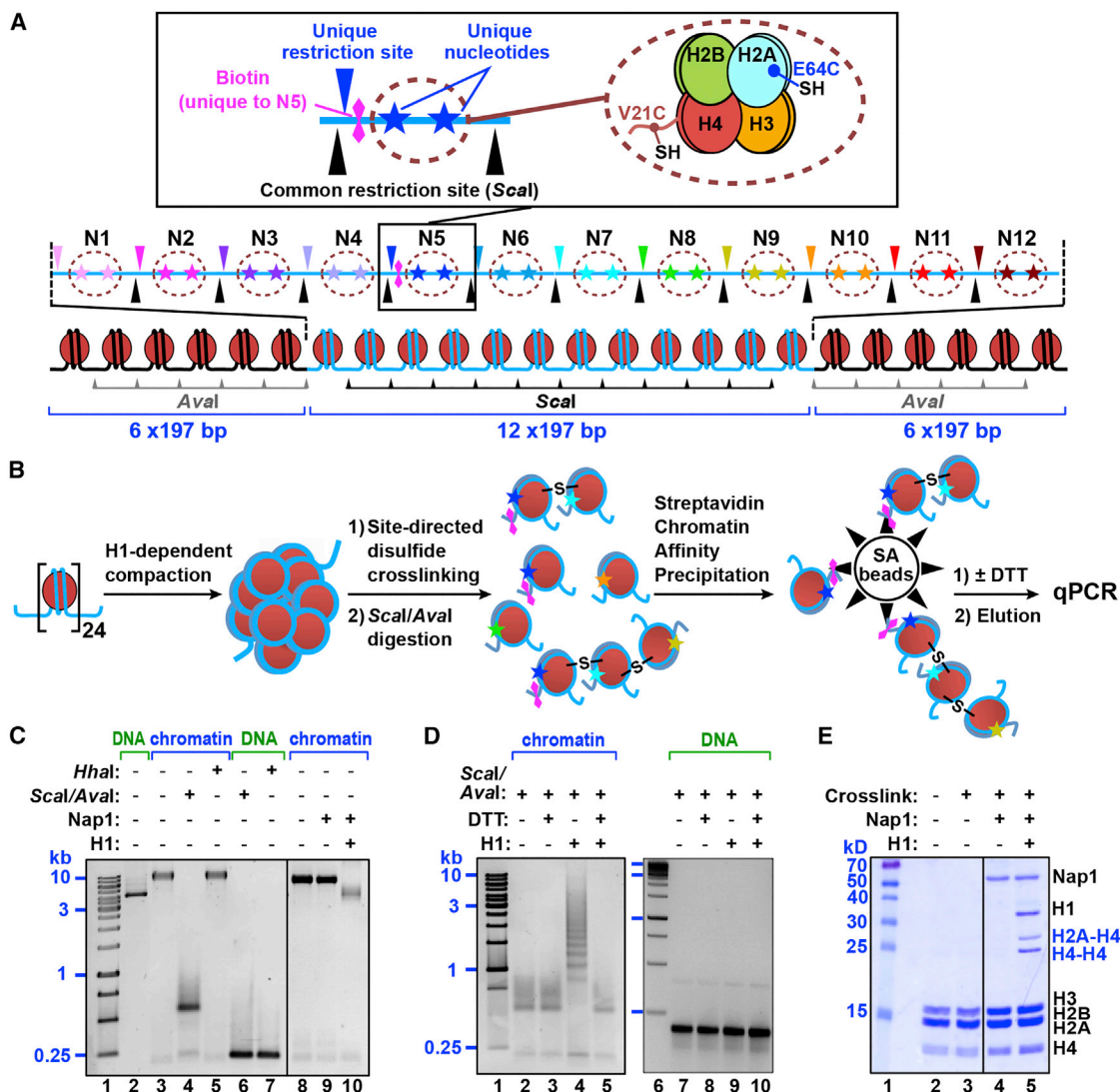
Figure 3. ICNN Analysis of Nucleosome Arrays

(A) Design of the 24-nucleosome array.

(B) ICNN protocol.

(C) Native agarose gel of the nucleosome array and of naked DNA treated with the indicated enzymes. Left: restriction digest. Cleavage of the ScaI and AvaI sites in the linker DNA (lane 4) and lack of cleavage of the HhaI site (lane 5) in the core DNA confirm the correct assembly and full nucleosome occupancy of the 24 × 197 bp DNA. Right: enhanced mobility of the 24-nucleosome array upon Nap1-mediated H1 deposition.

(D) Native agarose gel showing ScaI/AvaI digestion products of crosslinked nucleosome arrays (lanes 2–5) or of the DNA isolated from these arrays (lanes 7–10) following treatment with or without 100 mM DTT. ScaI/AvaI digestion revealed a ladder of at least six bands, all migrating more slowly than the mononucleosome (lane 4). Replacement of these bands with a mononucleosome band upon DTT treatment (lane 5) suggests that crosslinked species contained up to six or more nucleosomes tethered through disulfide bonds. Analysis of the DNA isolated from ScaI/AvaI-digested crosslinked arrays revealed only monomeric repeat 601 DNA, both for untreated and DTT-treated arrays, confirming that the digestion had gone to completion (lanes 7–10).

(E) SDS-PAGE (18%) of the indicated samples. As reported previously (Dorigo et al., 2004), bands corresponding to H4-H4 and H2A-H4 adducts were observed in the H1-bound arrays (lane 5) but not in arrays prepared without H1 (lane 4), reflecting the poor compaction of the latter arrays.

See also Figures S4 and S5.

with increasing numeric distance from the biotinylated nucleosome. These results confirm a two-start fiber organization with a type II interface on both sides of each nucleosome, strongly validating our 6-mer crystal structure. We note that the type II interface is also compatible with three additional H4-H2A and H4-H2B internucleosome crosslinks recently reported for a

12-nucleosome array in solution (Chen et al., 2017; Figures S4B and S4C).

The 6-mer Has an Extended Conformation in Solution

We next verified the 6-mer conformation in solution by small-angle X-ray scattering (SAXS). Scattering data were collected
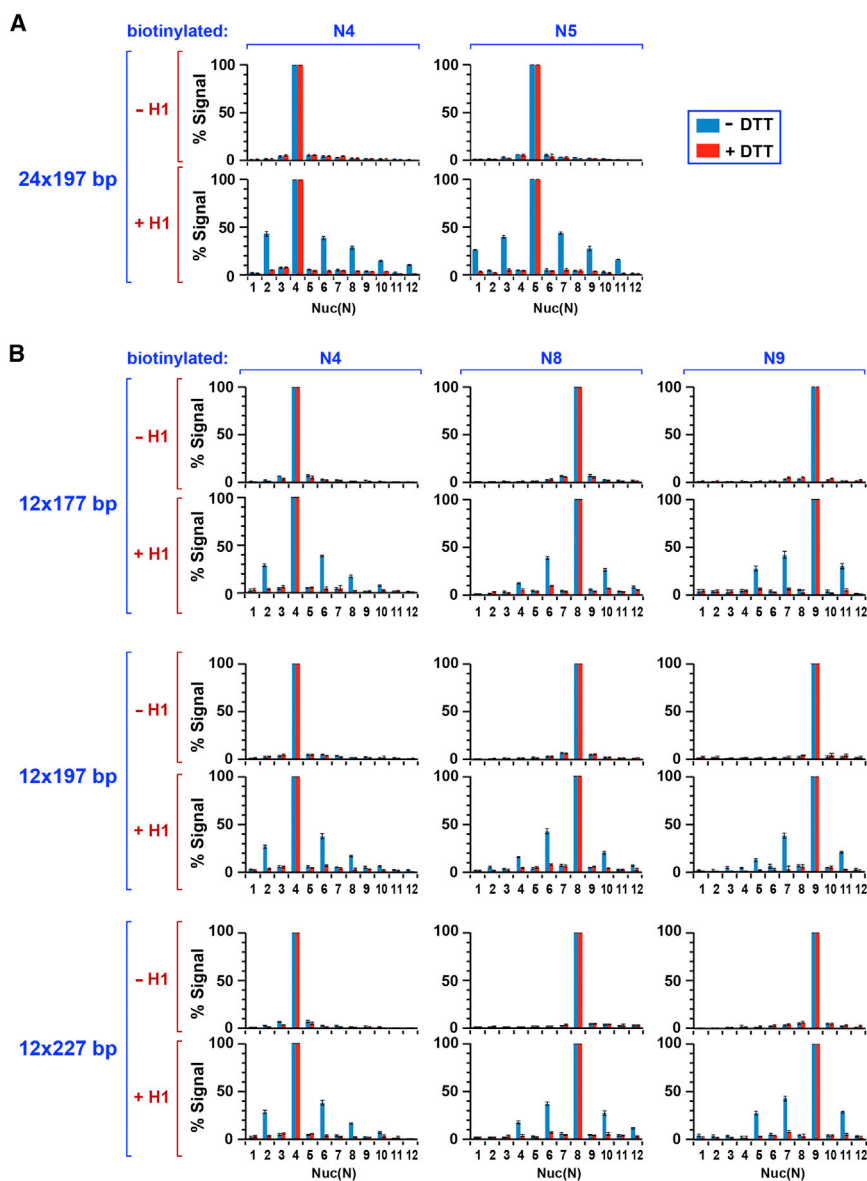
A

biotinylated:

24x197 bp

N4   N5

− H1

+ H1

% Signal (100, 50, 0 axes)

Nuc(N) 1 2 3 4 5 6 7 8 9 10 11 12

Legend: − DTT (blue), + DTT (red)

B

biotinylated: N4   N8   N9

12x177 bp

− H1

+ H1

12x197 bp

− H1

+ H1

12x227 bp

− H1

+ H1

% Signal (100, 50, 0 axes)

Nuc(N) 1 2 3 4 5 6 7 8 9 10 11 12

Figure 4. Evidence for a Two-Start Helix with Uniform Interfaces

(A) Specific qPCR signals measured for nucleosomes N1–N12 for a 24-nucleosome array biotinylated on either N4 (left) or N5 (right).

(B) ICNN results for 12-nucleosome arrays with repeat lengths of 177, 197, and 227 bp. Specific qPCR signals were measured for arrays biotinylated on either N4, N8, or N9, as indicated. Data are represented as mean ± SEM.

from 6 × 187 bp nucleosome arrays dialyzed against buffers containing 1, 50, or 90 mM NaCl (the last of these resembles the 6-mer crystallization conditions; Figure 5A). As expected, the observed scattering showed that the array became increasingly compact with increasing ionic strength, as evidenced by a decrease in the radius of gyration (R_g) and maximal diameter (D_{max}) (Figure 5B), a leftward shift in the distance probability distribution (Figure 5C), changes in the Kratky plot indicative of an increasing degree of order (Figure 5C, inset), and increasingly compact *ab initio* bead models (Figure 5D). The observed scattering and that predicted from our crystal structure became increasingly similar as the NaCl concentration increased, although they did not match perfectly at 90 mM NaCl (χ^2 = 2.54); indeed, the larger R_g and D_{max} values determined for the 90-mM dataset compared with those calculated from the crystal structure indicate a more extended conformation in solution

(Figures 5A and 5B). This finding is consistent with the *ab initio* bead model, into which the crystal structure can be snugly fitted but which includes additional beads outside of the fitted volume (Figure 5E). Importantly, the bead model exhibits a relatively flat shape resembling that of the untwisted array in the crystal.

To gain additional insights, we used analytical ultracentrifugation (AUC) to determine the sedimentation velocity of the 6-mer under various ionic conditions (Figure 5F). In 90 mM NaCl, the 6-mer sedimented with a velocity intermediate between that observed at 1 mM NaCl, where chromatin adopts a highly open conformation, and that observed in the presence of submillimolar $MgCl_2$, which efficiently compacts nucleosome arrays, confirming that the ionic conditions used for crystallization favor a partly condensed conformation. The average sedimentation coefficient for the 6-mer at 90 mM NaCl (33 S) was lower than that predicted from the crystal structure (36.2 S), confirming a more extended solution conformation. Thus, the combined SAXS and AUC results reveal that the 6-mer is incompletely condensed under the ionic conditions used for crystallization and becomes slightly more compact upon crystallization. Consequently, the lower nucleosome packing density of the 6-mer crystal structure relative to that of a 30-nm fiber is not a crystallization artifact but genuinely reflects an incomplete state of hexanucleosome compaction.

Cryo-EM Confirms an Untwisted Array Conformation

We next sought to observe nucleosome arrays under different ionic conditions by cryo-EM. As expected, the hexanucleosome adopts an open zigzag conformation in the presence of low (5 mM) NaCl (Figure 6, rows 1 and 2; Figure S6A). We could not obtain images for particles in the presence of higher (≥50 mM) NaCl concentrations because of excessive sample dissociation on the cryo-EM grid; however, samples behaved well in the presence of submillimolar $MgCl_2$. Notably, we observed particles in 0.35 mM $MgCl_2$ that show a striking
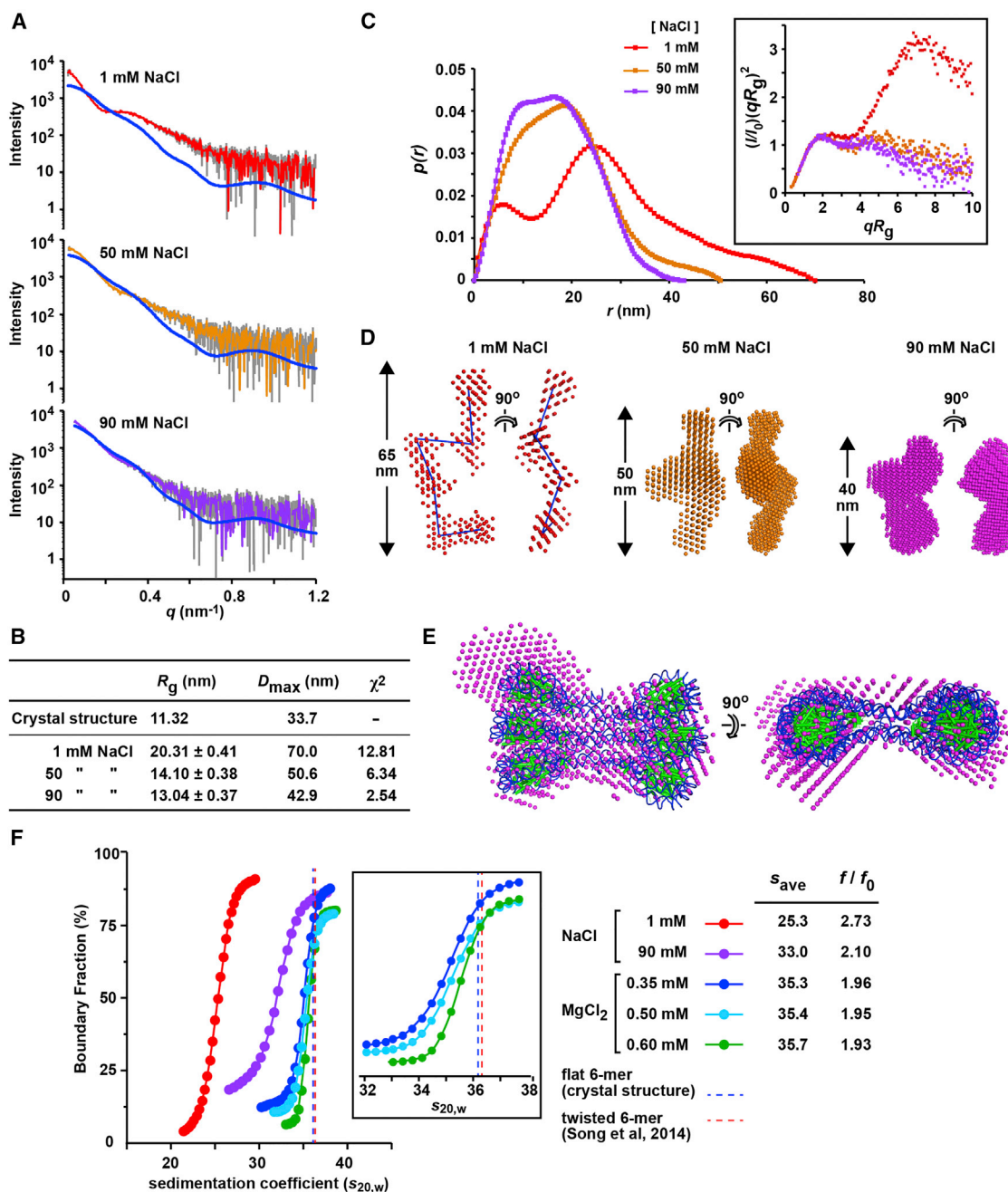
Figure 5. SAXS and AUC Analyses Confirm an Extended Conformation in Solution

(A) Scattering curves for 6-nucleosome arrays in 1, 50, or 90 mM NaCl. The scattering predicted from the 6-mer crystal structure is shown in blue.

(B) Summary of radius of gyration (R_g) and maximal diameter (D_{max}) values deduced from the observed scattering, together with χ^2 values for the fit with the scattering predicted from the crystal structure.

(C) Distance probability distributions. The double peak at 1 mM NaCl reflects the large separation between nucleosomes in an open zigzag conformation. Inset: normalized Kratky plots. The common peak at $qR_g = 1.7$ is characteristic of globular structures, consistent with the presence of well-folded nucleosomal units (Brennich et al., 2017). The increase at higher qR_g values for the 1 mM dataset indicates a highly flexible structure (Hammel, 2012).

(D) *Ab initio* bead models. The model at 1 mM NaCl presents six domains with center-to-center distances of 18–20 nm, consistent with an open zigzag conformation.

(E) Alignment of the 6-mer crystal structure with the *ab initio* model at 90 mM NaCl.

(F) Sedimentation velocity analysis of 6-nucleosome arrays prepared in buffers containing NaCl or $MgCl_2$ as indicated. The average sedimentation coefficient and frictional ratio (f/f_0) are indicated for the principal species sedimenting in the 20- to 40-S range. The inset shows an expanded view for the three samples measured in the presence of $MgCl_2$. Sedimentation coefficients predicted for the crystal structure and for the model of the twisted 6-mer are indicated by dashed lines.
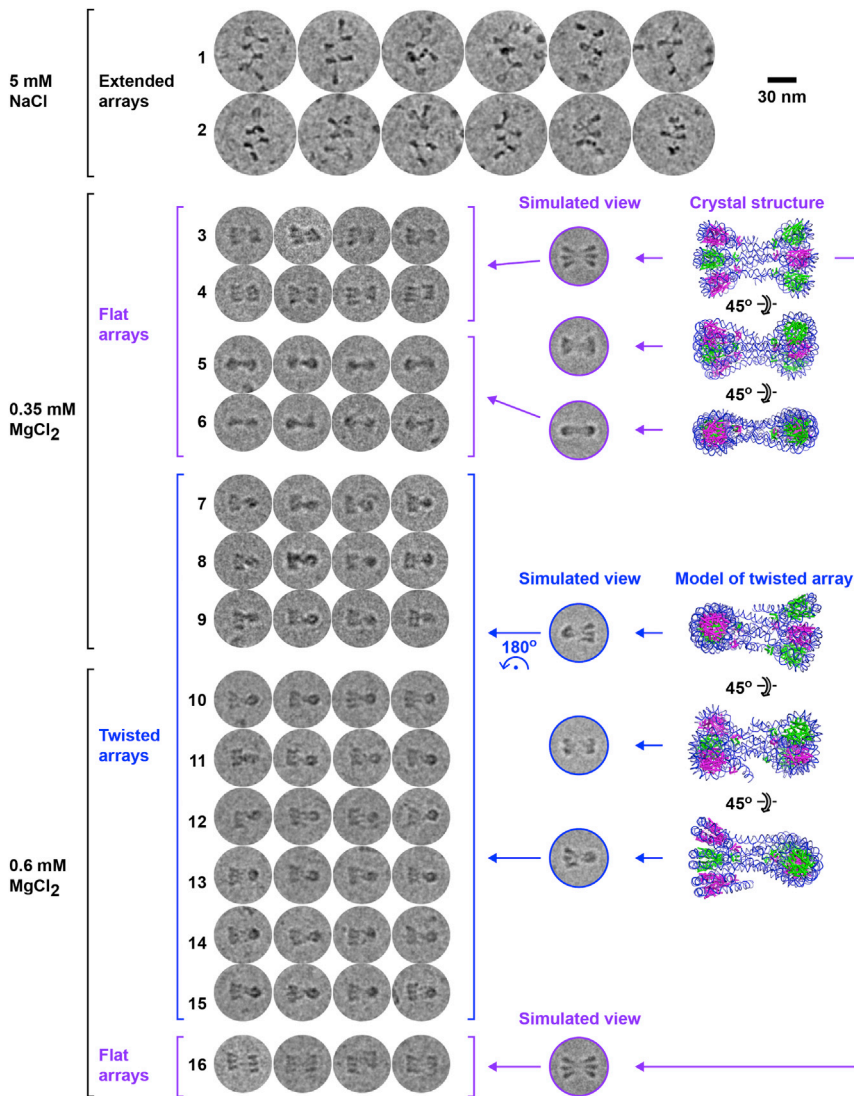
Figure 6. Cryo-EM Analysis Confirms a Flat Array Conformation and Reveals a Twisted Conformation Stabilized by Increased Mg^{2+}

Molecular images are shown for 6 × 187 bp nucleosome arrays dialyzed against 5 mM NaCl (top), 0.35 mM MgCl$_2$ (center), and 0.6 mM MgCl$_2$ (bottom). Images simulated from the 6-mer crystal structure and from a model of a twisted 6-mer are shown. In 0.35 mM MgCl$_2$, 53% and 31% of particles adopted a flat or twisted conformation, respectively, whereas 16% were misfolded or unfolded (145 particles in total). In 0.6 mM MgCl$_2$, the corresponding distribution was 8% flat, 73% twisted, and 19% mis- or unfolded (184 particles in total). See also Figures S6 and S7.

These images closely match views simulated from the model of a twisted 6-mer derived from nucleosomes N1–N6 of the condensed 12-mer. Thus, the flat and twisted 6-mer conformations appear to co-exist at 0.35 mM MgCl$_2$, with the flat conformation slightly more prevalent. Remarkably, increasing the MgCl$_2$ concentration to 0.6 mM resulted in cryo-EM images that almost exclusively exhibited particles in the twisted conformation, with only an occasional particle in the flat conformation (Figure 6, rows 10–16; Figure S6C). This finding agrees with our AUC data: increasing the MgCl$_2$ concentration from 0.35 to 0.6 mM yielded a small but detectable increase in average sedimentation coefficient (from 35.3 to 35.7 S), which correlates with the small shift in sedimentation coefficient predicted for a flat (36.2 S) versus a twisted (36.4 S) array (Figure 5F). We conclude that flat and twisted array conformations co-exist in solution and that a small increase in Mg^{2+} concentration shifts the conformational landscape toward the twisted state.

agreement with views simulated from our crystal structure (Figure 6, rows 3–6; Figure S6B). Specifically, particles with a ladder- or dumbbell-like appearance agree well with side and top views of the crystal structure, respectively, demonstrating that an untwisted array conformation is well-populated in solution. Extending the analysis to 12-nucleosome arrays also revealed particles with an open zigzag conformation at low NaCl concentration and a ladder-like conformation in the presence of 0.35–0.5 mM MgCl$_2$ (Figure S7), indicating that the untwisted array conformation is not limited to 6-mers but can also be adopted by longer arrays.

An Increase in Mg^{2+} Shifts the 6-mer to a Twisted Conformation

Besides particles with a ladder- or dumbbell-like shape, the cryo-EM images taken at 0.35 mM MgCl$_2$ also present particles with a chimeric appearance (half a ladder joined to half a dumbbell), suggesting that the two nucleosomal stacks are mutually orthogonally oriented (Figure 6, rows 7–9; and Figure S6B).

H1 Binds the 6-mer on the Dyad

In our crystal structure, each DNA linker exhibits a conformation closely resembling that in the H1-bound mononucleosome structure (at least for the core-proximal DNA helical turn; Bednar et al., 2017) and is sterically compatible with the on-dyad H1 binding mode observed in that structure (Figures 7A and S8A). To verify how H1 binds to a 6-nucleosome array, we mapped H1-DNA interactions at single-nucleotide resolution by hydroxyl radical footprinting under ionic conditions close to those used for crystallization. Each nucleosome within the array showed an identical H1-dependent footprint pattern as that reported for isolated nucleosomes (Syed et al., 2010; Bednar et al., 2017), exhibiting pronounced protection at the dyad and a 10-bp repeat pattern within the linker DNA (Figure 7B). Moreover, specific nucleotides protected at
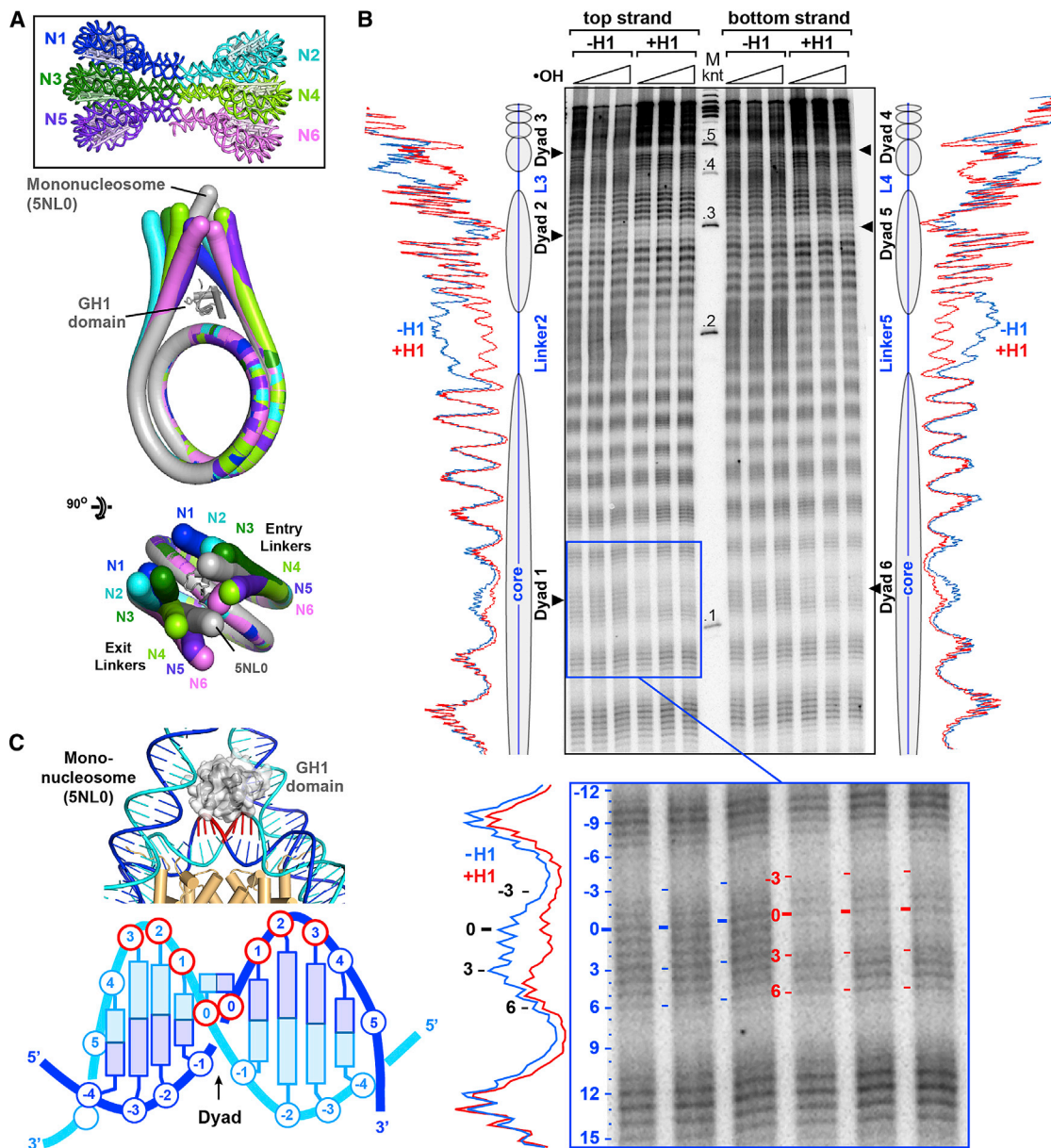
Figure 7. Footprinting Indicates that Histone H1 Binds on the Dyad

(A) The untwisted 6-mer is compatible with an on-dyad GH1 binding mode. The six nucleosomes of the array were each aligned with the structure of the H1-bound 197-bp mononucleosome (Bednar et al., 2017) (PDB: 5NL0). The mononucleosome DNA and GH1 domain are shown in gray.

(B) Hydroxyl radical footprinting analysis of a 6-nucleosome array. Arrowheads indicate regions of base protection of nucleotides located at the dyad in nucleosomes N1–N3 (left half) and N4–N6 (right half). Inset: magnified view of nucleotides around the dyad of nucleosome N1.

(C) View of the dyad region of the H1-bound 197-bp mononucleosome structure (Bednar et al., 2017). Nucleosomal core nucleotides within contact distance of the GH1 domain (in either dyad-related orientation) are indicated in red.

See also Figure S8.

the dyad agreed well with nucleotides in the H1-bound mononucleosome structure, which localize close to the globular H1 (GH1) domain (Figure 7C). Thus, the GH1 domain appears to adopt an on-dyad binding mode in the hexanucleosome. As noted previously (Bednar et al., 2017), the linker DNA conformation in the condensed 12-mer is unfavorable for on-dyad

binding. Conversely, our 6-mer crystal structure is sterically incompatible with the off-dyad binding mode observed in the condensed 12-mer (Figures S8B and S8C). These findings suggest that different fiber geometries with distinct linker DNA conformations may be characterized by alternate H1 binding modes.

DISCUSSION

In this study, we investigated H1-bound nucleosome arrays using a structural and biochemical approach. Our crystal structure of a hexanucleosome reveals a two-start helix characterized by a flat zigzag arrangement of nucleosomes, uniform type II nucleosome stacking interfaces, a nucleosome packing density nearly half of that reported for 30-nm chromatin fibers, and a core-proximal linker DNA conformation resembling that of an H1-bound mononucleosome. Our AUC and SAXS data confirm that, under the ionic conditions used for crystallization, the hexanucleosome adopts a flat, incompletely condensed conformation in solution. ICNN analyses of 12- and 24-nucleosome arrays show that nucleosome N_i is within disulfide crosslinking distance of nucleosomes $N_{i \pm 2}$, corroborating a two-start helical organization. Daisy chains of up to five crosslinked nucleosomes confirm type II interfaces on both sides of each nucleosome, strongly validating our 6-mer crystal structure. Type II stacking within the array appears to be contingent on H1 binding since no crosslinking was observed in the absence of H1. This is consistent with the observation that H1 stabilizes a more compact form of a 197-bp mononucleosome (Bednar et al., 2017): in the absence of H1, the two linker arms adopt a divergent geometry incompatible with the fiber geometry observed in the 6-mer crystal structure.

The above data lead us to propose a model for an extended chromatin fiber with a flat ladder-like conformation. Cryo-EM images of 6- and 12-nucleosome arrays match views simulated from our crystal structure and extended model, respectively, providing direct evidence for the ladder-like conformation in solution. Our crystal structure is strikingly different from the structure reported for a condensed 12-nucleosome array, which adopts a more compact, twisted conformation characterized by dimorphic nucleosome stacking interfaces, an off-dyad H1 binding mode, and a distinct DNA linker geometry (Song et al., 2014). Remarkably, our cryo-EM data revealed that, in the presence of submillimolar Mg^{2+}, the flat 6-nucleosome array co-exists with a twisted conformation resembling that adopted by nucleosomes N1–N6 of the condensed 12-mer. Moreover, a minor increase in Mg^{2+} levels preferentially stabilized the twisted conformation. These findings demonstrate, first, that the same linker histone can simultaneously associate with two distinct fiber conformations and, second, that the two fiber conformations exist in a dynamic equilibrium that can be shifted by a minor change in ionic environment.

Our cryo-EM data do not allow us to determine whether the twisted arrays observed in the presence of Mg^{2+} have uniform or dimorphic stacking interfaces; hence, their precise conformation might differ somewhat from that reported for the condensed 12-mer of Song et al. (2014). Curiously, the latter structure was determined from glutaraldehyde-fixed nucleosome arrays under low-salt conditions, that according to our findings, should favor a less compact, untwisted conformation. A possible explanation for this discrepancy comes from a recent study showing that glutaraldehyde perturbs nucleosome array conformation (Zhou et al., 2018), raising the possibility that glutaraldehyde mimics the effects of Mg^{2+} on chromatin fiber structure.

Our results suggest that the untwisted array represents a plausible intermediate along the assembly (or disassembly) pathway of the condensed 30-nm fiber, whereby nucleosomes initially self-associate into two parallel stacks to attain a partly condensed state (as shown in Figure 2B) and the two stacks subsequently twist around each other to generate a more compact fiber (as shown in Figure 2A) (or the inverse of these steps during disassembly). Our footprinting data show that, under ionic conditions favoring the flat array conformation, H1 associates with the 6-mer in an on-dyad mode, whereas an off-dyad mode is observed for the condensed 12-mer (Song et al., 2014). This suggests that a switch between partly and fully condensed fiber conformations is associated with a change in H1 binding configuration. This hypothesis is supported by computational studies showing that the H1 binding mode is influenced by the conformational dynamics of the linker DNA and the local nucleosome environment (Öztürk et al., 2016; Perišić and Schlick, 2017). Further studies, including high-resolution structures of H1-bound nucleosome arrays in both the flat and twisted conformations, are required to verify this hypothesis.

Interestingly, modeling shows that GH1 domains bound on the dyads of an untwisted array are too far apart to interact with one another, whereas the off-dyad GH1 domains bound on either side of a type II interface in the condensed 12-mer are juxtaposed and presumed to interact (Song et al., 2014; Figure S8D). Such GH1-GH1 interactions could contribute significantly to the stability of a given nucleosome array conformation and thus be a potential target for regulation. Indeed, the GH1 domain contains numerous residues that undergo post-translational modifications (PTMs) (e.g., Wisniewski et al., 2007) that could conceivably modulate GH1-GH1 interactions. In this connection, a recent study investigating the dynamic acetylation of H1 on residue Lys85 (located in the GH1 domain) in response to DNA damage reported that the acetylation mimic mutant H1K85Q dramatically increased the sedimentation rate of reconstituted nucleosome arrays and favored chromatin condensation in cells (Li et al., 2018). It is tempting to speculate that K85 acetylation or Gln substitution induces H1 to adopt a different nucleosome binding mode that favors a more compact fiber conformation. In line with this idea, point mutations introduced onto the surface of chicken GH5 induced the binding mode to switch from on- to off-dyad (Zhou et al., 2016), while a recent computational study confirmed the sensitivity of the linker histone binding mode to single-point mutations and PTMs (Öztürk et al., 2018).

Similarly, H1 may mediate additional interactions with chromatin-binding factors or other nucleosomal components that could influence (or be influenced by) the chromatin fiber conformation and thereby offer further potential for regulation. Indeed, a recent study showed that the dynamics of histone H3 tails and their susceptibility to PTMs are reduced by H1 binding; this effect is dependent on the H1 C-terminal domain and mediated by direct interactions between the H3 tail and linker DNA (Stützer et al., 2016). Direct coupling between H3 tail and linker DNA dynamics explains why H1 reduces H3 tail dynamics since H1 directly reduces linker DNA dynamics (Pachov et al., 2011; Bednar et al., 2017). Because the flat and twisted nucleosome array conformations have different linker DNA trajectories, they could conceivably interact differently with the H3 tails and

thereby confer differential susceptibility to PTMs. Conversely, different H3 PTMs might favor different interaction modes with the linker DNA and selectively stabilize different chromatin fiber conformations.

In summary, our findings reveal a flat chromatin fiber conformation that can switch to a twisted conformation upon a shift in ionic environment, suggesting a possible folding pathway for a compact 30-nm fiber. We speculate that the salt-dependent changes in nucleosome array structure that we observe *in vitro* reflect conformational fluctuations that specific regulatory processes could exploit *in vivo* to allow chromatin to switch between different states of compaction in response to a change in the local environment. More generally, our study highlights the diversity of fiber structures that nucleosome arrays can adopt, providing insights into the conformational plasticity of chromatin that is central to diverse gene-regulatory processes.

STAR★METHODS

Detailed methods are provided in the online version of this paper and include the following:

- KEY RESOURCES TABLE
- CONTACT FOR REAGENT AND RESOURCE SHARING
- EXPERIMENTAL MODEL AND SUBJECT DETAILS
- METHOD DETAILS
  - Identification of Closest Neighbor Nucleosome (ICNN)
  - Preparation of hexanucleosome array for crystal structure determination
  - Hydroxyl-radical footprinting analysis of a hexanucleosome array
  - Crystal structure determination and analysis
  - Cryo-electron microscopy
  - Small-angle scattering
  - Analytical ultracentrifugation
- QUANTIFICATION AND STATISTICAL ANALYSIS
- DATA AND SOFTWARE AVAILABILITY

REFERENCES

Adams, P.D., Afonine, P.V., Bunkóczi, G., Chen, V.B., Davis, I.W., Echols, N., Headd, J.J., Hung, L.W., Kapral, G.J., Grosse-Kunstleve, R.W., et al. (2010). PHENIX: a comprehensive Python-based system for macromolecular structure solution. Acta Crystallogr. D Biol. Crystallogr. *66*, 213–221.

Allahverdi, A., Chen, Q., Korolev, N., and Nordenskiöld, L. (2015). Chromatin compaction under mixed salt conditions: opposite effects of sodium and potassium ions on nucleosome array folding. Sci. Rep. *5*, 8512.

Bednar, J., Horowitz, R.A., Grigoryev, S.A., Carruthers, L.M., Hansen, J.C., Koster, A.J., and Woodcock, C.L. (1998). Nucleosomes, linker DNA, and linker histone form a unique structural motif that directs the higher-order folding and compaction of chromatin. Proc. Natl. Acad. Sci. USA *95*, 14173–14178.

Bednar, J., Garcia-Saez, I., Boopathi, R., Cutter, A.R., Papai, G., Reymer, A., Syed, S.H., Lone, I.N., Tonchev, O., Crucifix, C., et al. (2017). Structure and dynamics of a 197 bp nucleosome in complex with linker histone H1. Mol. Cell *66*, 384–397.e8.

Belmont, A.S., and Bruce, K. (1994). Visualization of G1 chromosomes: a folded, twisted, supercoiled chromonema model of interphase chromatid structure. J. Cell Biol. *127*, 287–302.

Belmont, A.S., Sedat, J.W., and Agard, D.A. (1987). A three-dimensional approach to mitotic chromosome structure: evidence for a complex hierarchical organization. J. Cell Biol. *105*, 77–92.

Bilokapic, S., Strauss, M., and Halic, M. (2018). Cryo-EM of nucleosome core particle interactions in trans. Sci. Rep. *8*, 7046.

Brennich, M.E., Kieffer, J., Bonamis, G., De Maria Antolinos, A., Hutin, S., Pernot, P., and Round, A. (2016). Online data analysis at the ESRF bioSAXS beamline, BM29. J. Appl. Cryst. *49*, 203–212.

Brennich, M., Pernot, P., and Round, A. (2017). How to analyze and present SAS Data for publication. Adv. Exp. Med. Biol. *1009*, 47–64.

Butler, P.J., and Thomas, J.O. (1980). Changes in chromatin folding in solution. J. Mol. Biol. *140*, 505–529.

Cai, S., Böck, D., Pilhofer, M., and Gan, L. (2018). The in situ structures of mono-, di-, and tri-nucleosomes in human heterochromatin. bioRxiv. https://doi.org/10.1101/334490.

Caterino, T.L., Fang, H., and Hayes, J.J. (2011). Nucleosome linker DNA contacts and induces specific folding of the intrinsically disordered H1 carboxyl-terminal domain. Mol. Cell. Biol. *31*, 2341–2348.

Chen, Q., Yang, R., Korolev, N., Liu, C.F., and Nordenskiöld, L. (2017). Regulation of nucleosome stacking and chromatin compaction by the histone H4 N-terminal tail-H2A acidic patch interaction. J. Mol. Biol. *429*, 2075–2092.

Chua, E.Y., Vasudevan, D., Davey, G.E., Wu, B., and Davey, C.A. (2012). The mechanics behind DNA sequence-dependent properties of the nucleosome. Nucleic Acids Res. *40*, 6338–6352.

Collepardo-Guevara, R., and Schlick, T. (2014). Chromatin fiber polymorphism triggered by variations of DNA linker lengths. Proc. Natl. Acad. Sci. USA *111*, 8061–8066.

Dorigo, B., Schalch, T., Kulangara, A., Duda, S., Schroeder, R.R., and Richmond, T.J. (2004). Nucleosome arrays reveal the two-start organization of the chromatin fiber. Science *306*, 1571–1573.

Ekundayo, B., Richmond, T.J., and Schalch, T. (2017). Capturing Structural Heterogeneity in Chromatin Fibers. J. Mol. Biol. *429*, 3031–3042.

Eltsov, M., Maclellan, K.M., Maeshima, K., Frangakis, A.S., and Dubochet, J. (2008). Analysis of cryo-electron microscopy images does not support the existence of 30-nm chromatin fibers in mitotic chromosomes in situ. Proc. Natl. Acad. Sci. USA *105*, 19732–19737.

Emsley, P., Lohkamp, B., Scott, W.G., and Cowtan, K. (2010). Features and development of Coot. Acta Crystallogr. D Biol. Crystallogr. *66*, 486–501.

Evans, P. (2006). Scaling and assessment of data quality. Acta Crystallogr. D Biol. Crystallogr. *62*, 72–82.

Finch, J.T., and Klug, A. (1976). Solenoidal model for superstructure in chromatin. Proc. Natl. Acad. Sci. USA *73*, 1897–1901.

Fussner, E., Strauss, M., Djuric, U., Li, R., Ahmed, K., Hart, M., Ellis, J., and Bazett-Jones, D.P. (2012). Open and closed domains in the mouse genome are configured as 10-nm chromatin fibres. EMBO Rep. *13*, 992–996.

Gan, L., Ladinsky, M.S., and Jensen, G.J. (2013). Chromatin in a marine picoeukaryote is a disordered assemblage of nucleosomes. Chromosoma *122*, 377–386.

Gerchman, S.E., and Ramakrishnan, V. (1987). Chromatin higher-order structure studied by neutron scattering and scanning transmission electron microscopy. Proc. Natl. Acad. Sci. USA *84*, 7802–7806.

Greulich, K.O., Wachtel, E., Ausio, J., Seger, D., and Eisenberg, H. (1987). Transition of chromatin from the "10 nm" lower order structure, to the "30 nm" higher order structure as followed by small angle X-ray scattering. J. Mol. Biol. *193*, 709–721.

Griffith, J.D. (1975). Chromatin structure: deduced from a minichromosome. Science *187*, 1202–1203.

Grigoryev, S.A., Arya, G., Correll, S., Woodcock, C.L., and Schlick, T. (2009). Evidence for heteromorphic chromatin fibers from analysis of nucleosome interactions. Proc. Natl. Acad. Sci. USA *106*, 13317–13322.

Grigoryev, S.A., Bascom, G., Buckwalter, J.M., Schubert, M.B., Woodcock, C.L., and Schlick, T. (2016). Hierarchical looping of zigzag nucleosome chains in metaphase chromosomes. Proc. Natl. Acad. Sci. USA *113*, 1238–1243.

Hammel, M. (2012). Validation of macromolecular flexibility in solution by small-angle X-ray scattering (SAXS). Eur. Biophys. J. *41*, 789–799.

Hansen, J.C., Ausio, J., Stanik, V.H., and van Holde, K.E. (1989). Homogeneous reconstituted oligonucleosomes, evidence for salt-dependent folding in the absence of histone H1. Biochemistry *28*, 9129–9136.

Hsieh, T.H., Weiner, A., Lajoie, B., Dekker, J., Friedman, N., and Rando, O.J. (2015). Mapping Nucleosome Resolution Chromosome Folding in Yeast by Micro-C. Cell *162*, 108–119.

Kabsch, W. (1976). Solution for best rotation to relate 2 sets of vectors. Acta Crystallogr. A *32*, 922–923.

Kabsch, W. (2010). XDS. Acta Crystallogr. D Biol. Crystallogr. *66*, 125–132.

Kizilyaprak, C., Spehner, D., Devys, D., and Schultz, P. (2010). In vivo chromatin organization of mouse rod photoreceptors correlates with histone modifications. PLoS ONE *5*, e11039.

Konarev, P.V., Volkov, V.V., Sokolova, A.V., Koch, M.H.J., and Svergun, D.I. (2003). PRIMUS - a Windows-PC based system for small-angle scattering data analysis. J. Appl. Cryst. *36*, 1277–1282.

Korolev, N., Allahverdi, A., Yang, Y., Fan, Y., Lyubartsev, A.P., and Nordenskiöld, L. (2010). Electrostatic origin of salt-induced nucleosome array compaction. Biophys. J. *99*, 1896–1905.

Korolev, N., Lyubartsev, A.P., and Nordenskiöld, L. (2018). A systematic analysis of nucleosome core particle and nucleosome-nucleosome stacking structure. Sci. Rep. *8*, 1543.

Langmore, J.P., and Schutt, C. (1980). The higher order structure of chicken erythrocyte chromosomes in vivo. Nature *288*, 620–622.

Li, Y., Li, Z., Dong, L., Tang, M., Zhang, P., Zhang, C., Cao, Z., Zhu, Q., Chen, Y., Wang, H., et al. (2018). Histone H1 acetylation at lysine 85 regulates chromatin condensation and genome stability upon DNA damage. Nucleic Acids Res. *46*, 7716–7730.

Lowary, P.T., and Widom, J. (1998). New DNA sequence rules for high affinity binding to histone octamer and sequence-directed nucleosome positioning. J. Mol. Biol. *276*, 19–42.

Luger, K., Mäder, A.W., Richmond, R.K., Sargent, D.F., and Richmond, T.J. (1997). Crystal structure of the nucleosome core particle at 2.8 A resolution. Nature *389*, 251–260.

Makarov, V.L., Dimitrov, S.I., and Petrov, P.T. (1983). Salt-induced conformational transitions in chromatin. A flow linear dichroism study. Eur. J. Biochem. *133*, 491–497.

Marion, C., and Roux, B. (1978). Nucleosomes arrangement in chromatin. Nucleic Acids Res. *5*, 4431–4449.

McCoy, A.J., Grosse-Kunstleve, R.W., Adams, P.D., Winn, M.D., Storoni, L.C., and Read, R.J. (2007). Phaser crystallographic software. J. Appl. Cryst. *40*, 658–674.

Nishino, Y., Eltsov, M., Joti, Y., Ito, K., Takata, H., Takahashi, Y., Hihara, S., Frangakis, A.S., Imamoto, N., Ishikawa, T., and Maeshima, K. (2012). Human mitotic chromosomes consist predominantly of irregularly folded nucleosome fibres without a 30-nm chromatin structure. EMBO J. *31*, 1644–1653.

Ou, H.D., Phan, S., Deerinck, T.J., Thor, A., Ellisman, M.H., and O'Shea, C.C. (2017). ChromEMT: Visualizing 3D chromatin structure and compaction in interphase and mitotic cells. Science *357*, eaag0025.

Öztürk, M.A., Pachov, G.V., Wade, R.C., and Cojocaru, V. (2016). Conformational selection and dynamic adaptation upon linker histone binding to the nucleosome. Nucleic Acids Res. *44*, 6599–6613.

Öztürk, M.A., Cojocaru, V., and Wade, R.C. (2018). Dependence of chromatosome structure on linker histone sequence and posttranslational modification. Biophys. J. *114*, 2363–2375.

Pachov, G.V., Gabdoulline, R.R., and Wade, R.C. (2011). On the structure and dynamics of the complex of the nucleosome and the linker histone. Nucleic Acids Res. *39*, 5255–5263.

Perišić, O., and Schlick, T. (2017). Dependence of the linker histone and chromatin condensation on the nucleosome environment. J. Phys. Chem. B *121*, 7823–7832.

Petersen, M.T., Jonson, P.H., and Petersen, S.B. (1999). Amino acid neighbours and detailed conformational analysis of cysteines in proteins. Protein Eng. *12*, 535–548.

Ricci, M.A., Manzo, C., García-Parajo, M.F., Lakadamyali, M., and Cosma, M.P. (2015). Chromatin fibers are formed by heterogeneous groups of nucleosomes in vivo. Cell *160*, 1145–1158.

Ris, H., and Kubai, D.F. (1970). Chromosome structure. Annu. Rev. Genet. *4*, 263–294.

Risca, V.I., Denny, S.K., Straight, A.F., and Greenleaf, W.J. (2017). Variable chromatin structure revealed by in situ spatially correlated DNA cleavage mapping. Nature *541*, 237–241.

Robinson, P.J., Fairall, L., Huynh, V.A., and Rhodes, D. (2006). EM measurements define the dimensions of the "30-nm" chromatin fiber: evidence for a compact, interdigitated structure. Proc. Natl. Acad. Sci. USA *103*, 6506–6511.

Roulland, Y., Ouararhni, K., Naidenov, M., Ramos, L., Shuaib, M., Syed, S.H., Lone, I.N., Boopathi, R., Fontaine, E., Papai, G., et al. (2016). The flexible ends of CENP-A nucleosome are required for mitotic fidelity. Mol. Cell 63, 674–685.

Schalch, T., Duda, S., Sargent, D.F., and Richmond, T.J. (2005). X-ray structure of a tetranucleosome and its implications for the chromatin fibre. Nature 436, 138–141.

Scheffer, M.P., Eltsov, M., and Frangakis, A.S. (2011). Evidence for short-range helical order in the 30-nm chromatin fibers of erythrocyte nuclei. Proc. Natl. Acad. Sci. USA 108, 16992–16997.

Scheffer, M.P., Eltsov, M., Bednar, J., and Frangakis, A.S. (2012). Nucleosomes stacked with aligned dyad axes are found in native compact chromatin in vitro. J. Struct. Biol. 178, 207–214.

Song, F., Chen, P., Sun, D., Wang, M., Dong, L., Liang, D., Xu, R.M., Zhu, P., and Li, G. (2014). Cryo-EM study of the chromatin fiber reveals a double helix twisted by tetranucleosomal units. Science 344, 376–380.

Stützer, A., Liokatis, S., Kiesel, A., Schwarzer, D., Sprangers, R., Söding, J., Selenko, P., and Fischle, W. (2016). Modulations of DNA contacts by linker histones and post-translational modifications determine the mobility and modifiability of nucleosomal H3 tails. Mol. Cell 61, 247–259.

Svergun, D.I. (1992). Determination of the regularization parameter in indirect-transform methods using perceptual criteria. J. Appl. Cryst. 25, 495–503.

Svergun, D.I. (1999). Restoring low resolution structure of biological macromolecules from solution scattering using simulated annealing. Biophys. J. 76, 2879–2886.

Svergun, D., Barberato, C., and Koch, M.H. (1995). CRYSOL—a program to evaluate X-ray solution scattering of biological macromolecules from atomic coordinates. J. Appl. Cryst. 28, 768–773.

Syed, S.H., Goutte-Gattat, D., Becker, N., Meyer, S., Shukla, M.S., Hayes, J.J., Everaers, R., Angelov, D., Bednar, J., and Dimitrov, S. (2010). Single-base resolution mapping of H1-nucleosome interactions and 3D organization of the nucleosome. Proc. Natl. Acad. Sci. USA 107, 9620–9625.

Tachiwana, H., Kagawa, W., Shiga, T., Osakabe, A., Miya, Y., Saito, K., Hayashi-Takanaka, Y., Oda, T., Sato, M., Park, S.Y., et al. (2011). Crystal structure of the human centromeric nucleosome containing CENP-A. Nature 476, 232–235.

Terwilliger, T.C., Grosse-Kunstleve, R.W., Afonine, P.V., Moriarty, N.W., Adams, P.D., Read, R.J., Zwart, P.H., and Hung, L.W. (2008). Iterative-build OMIT maps: map improvement by iterative model building and refinement without model bias. Acta Crystallogr. D Biol. Crystallogr. 64, 515–524.

Thoma, F., Koller, T., and Klug, A. (1979). Involvement of histone H1 in the organization of the nucleosome and of the salt-dependent superstructures of chromatin. J. Cell Biol. 83, 403–427.

Tolstorukov, M.Y., Colasanti, A.V., McCandlish, D.M., Olson, W.K., and Zhurkin, V.B. (2007). A novel roll-and-slide mechanism of DNA folding in chromatin: implications for nucleosome positioning. J. Mol. Biol. 371, 725–738.

Vasudevan, D., Chua, E.Y., and Davey, C.A. (2010). Crystal structures of nucleosome core particles containing the '601' strong positioning sequence. J. Mol. Biol. 403, 1–10.

Volkov, V.V., and Svergun, D.I. (2003). Uniqueness of ab initio shape determination in small-angle scattering. J. Appl. Cryst. 36, 860–864.

Williams, S.P., Athey, B.D., Muglia, L.J., Schappe, R.S., Gough, A.H., and Langmore, J.P. (1986). Chromatin fibers are left-handed double helices with diameter and mass per unit length that depend on linker length. Biophys. J. 49, 233–248.

Wisniewski, J.R., Zougman, A., Krüger, S., and Mann, M. (2007). Mass spectrometric mapping of linker histone H1 variants reveals multiple acetylations, methylations, and phosphorylation as well as differences between cell culture and tissue. Mol. Cell. Proteomics 6, 72–87.

Woodcock, C.L. (1994). Chromatin fibers observed in situ in frozen hydrated sections. Native fiber diameter is not correlated with nucleosome repeat length. J. Cell Biol. 125, 11–19.

Woodcock, C.L., Frado, L.L., and Rattner, J.B. (1984). The higher-order structure of chromatin: evidence for a helical ribbon arrangement. J. Cell Biol. 99, 42–52.

Worcel, A., Strogatz, S., and Riley, D. (1981). Structure of chromatin and the linking number of DNA. Proc. Natl. Acad. Sci. USA 78, 1461–1465.

Zhou, B.R., Feng, H., Kato, H., Dai, L., Yang, Y., Zhou, Y., and Bai, Y. (2013). Structural insights into the histone H1-nucleosome complex. Proc. Natl. Acad. Sci. USA 110, 19390–19395.

Zhou, B.R., Jiang, J., Feng, H., Ghirlando, R., Xiao, T.S., and Bai, Y. (2015). Structural mechanisms of nucleosome recognition by linker histones. Mol. Cell 59, 628–638.

Zhou, B.R., Feng, H., Ghirlando, R., Li, S., Schwieters, C.D., and Bai, Y. (2016). A small number of residues can determine if linker histones are bound on or off dyad in the chromatosome. J. Mol. Biol. 428, 3948–3959.

Zhou, B.R., Jiang, J., Ghirlando, R., Norouzi, D., Sathish Yadav, K.N., Feng, H., Wang, R., Zhang, P., Zhurkin, V., and Bai, Y. (2018). Revisit of Reconstituted 30-nm Nucleosome Arrays Reveals an Ensemble of Dynamic Structures. J. Mol. Biol. 430 (18 Pt B), 3093–3110.

STAR★METHODS

KEY RESOURCES TABLE

REAGENT or RESOURCE	SOURCE	IDENTIFIER
Bacterial and Virus Strains		
One Shot BL21(DE3) Chemically Competent *E. coli*	Thermo Fischer Scientific	Cat# C600003
E.coli (BL21(DE3))	NEB	Cat# C2527H
Chemicals, Peptides, and Recombinant Proteins		
Recombinant *Xenopus laevis* core histones	Syed et al., 2010	N/A
	Caterino et al., 2011	
Recombinant human histones	Tachiwana et al., 2011	N/A
X. laevis linker histone H1.0b	Syed et al., 2010	N/A
	Caterino et al., 2011	
His-tagged NAP-1	Syed et al., 2010	N/A
Recombinant *Xenopus laevis* mutant histones	Roulland et al., 2016	N/A
Critical Commercial Assays		
Quant-iT PicoGreen dsDNA assay kit	Invitrogen/Thermo Fisher Scientific	Cat# P11496
Fast Start Universal SYBR Green Master	Roche/Sigma-Aldrich	Cat# 04913850001
Deposited Data		
Atomic coordinates of the 6 × 187 bp hexanucleosomal array bound to linker histone H1.0b	This paper	PDB: 6HKT
Crosslinking and hydroxyl-radical footprinting data	This paper; Mendeley Data	https://doi.org/10.17632/348t5n4m6k.1
Oligonucleotides		
197 bp Widom 601 DNA	Syed et al., 2010	N/A
187 bp Widom 601 DNA	Chua et al., 2012	N/A
Biotinylated repeat primers (N4):	This paper	N/A
Forward: 5′CATCAGTACTAGGTCTT CGAACAATACATGC**A**CAGGATGTA 3′		
Reverse: 5′GTGCATGTATTGACAT ATGACCTAGTACTGA**T**GGACCCTATACG 3′		
Biotinylated repeat primers (N5):	This paper	N/A
Forward:		
5′CTAGGTCATATGTCAAT ACATGC**A**CAGGATG 3′		
Reverse: 5′TATTGAACGTGCACCT AGTACTGA**T**GGACCCTATACGC 3′		
Recombinant DNA		
6 × 197 bp (wildtype 601)	This paper	N/A
12 × 197 bp (wildtype 601)	This paper	N/A
24 × 197 bp (wildtype 601) carrier DNA	This paper	N/A
24 × 197 bp (wildtype 601) (N1-N12) DNA	This paper	N/A
24 × 197 bp (wildtype 601) (N1-N12) DNA biotinylated on repeat N4 or N5	This paper	N/A
6 × 187 bp (wildtype 601)	This paper	N/A
pGEM-T-easy plasmid	Promega	Cat# A1360

Continued

REAGENT or RESOURCE	SOURCE	IDENTIFIER
Software and Algorithms		
XDS	Kabsch, 2010	http://homes.mpimf-heidelberg.mpg.de/~kabsch/xds/
AIMLESS (CCP4 supported program)	Evans, 2006	http://www.ccp4.ac.uk/dist/html/aimless.html
Phaser (CCP4 supported program)	McCoy et al., 2007	http://www.phaser.cimr.cam.ac.uk/index.php/Phaser_Crystallographic_Software
Phenix	Adams et al., 2010	https://www.phenix-online.org
Coot	Emsley et al., 2010	https://www2.mrc-lmb.cam.ac.uk/personal/pemsley/coot/
Lsqkab (CCP4 supported program)	Kabsch, 1976	http://www.ccp4.ac.uk/html/lsqkab.html
PRIMUS	Konarev et al., 2003	https://www.embl-hamburg.de/biosaxs/primus.html
GNOM	Svergun, 1992	https://www.embl-hamburg.de/biosaxs/gnom.html
DAMMIN	Svergun, 1999	https://www.embl-hamburg.de/biosaxs/dammin.html
DAMAVER	Volkov and Svergun, 2003	https://www.embl-hamburg.de/biosaxs/damaver.html
CRYSOL	Svergun et al., 1995	https://www.embl-hamburg.de/biosaxs/crysol.html
REDATE v 1.0.1.		http://biophysics.swmed.edu/MBR/software.html
SEDFIT v 14.1		http://www.analyticalultracentrifugation.com/download.htm
Gussi 1.2.1.		http://biophysics.swmed.edu/MBR/software.html
SEDNTERP v20130813 Beta		http://www.jphilo.mailway.com/download.htm
Ultrascan SOMO Revision: 3087		http://somo.aucsolutions.com
Adobe Photoshop version 12.0		https://www.adobe.com/products/photoshop.html
Other		
Model 491 Prep Cell	BioRad	Cat# 1702927
C-flat 2/2-2C Holey Carbon grid	EMS	Cat# CF-222C-25
Quantifoil R1.2/1.3 on Cu 200 mesh	EMS	Cat# Q2100CR1.3
Dynabeads M-280 Streptavidin	Invitrogen/Thermo Fisher Scientific	Cat# 11205D
CelluSepT2 dialysis Tubings - 6000 Da (10mm width)	Interchim	Cat# T2-10-15
Corning 96-well Black Flat Bottom Polystyrene NBS Microplate,	Corning	Cat# 3991
qPCR 96-well plate sub-skirted, low profile, frosted (ABI FAST systems)	Eurogentec	Cat# RT-PL96-AF

CONTACT FOR REAGENT AND RESOURCE SHARING

Further information and requests for resources and reagents should be directed to and will be fulfilled by the Lead Contact, Stefan Dimitrov (stefan.dimitrov@univ-grenoble-alpes.fr).

EXPERIMENTAL MODEL AND SUBJECT DETAILS

Histones and NAP-1 were overexpressed using BL21(DE3) competent *Escherichia coli* (Thermo Fisher Scientific and NEB) as previously described (Syed et al., 2010; Caterino et al., 2011; Tachiwana et al., 2011).

METHOD DETAILS

Identification of Closest Neighbor Nucleosome (ICNN)
Generation of 24 × 197 bp (wild-type 601) carrier DNA

The 601 Widom DNA (ATCGATGGACCCTATACGCGGCCGCCCTGGAGAATCCCGGTGCCGAGGCCGCTCAATTGGTCGTAGACA GCTCTAGCACCGCTTAAACGCACGTACGCGCTGTCCCCCGCGTTTTAACCGCCAAGGGGATTACTCCCTAGTCTCCAGGCACGTG TCAGATATATACATCCTGTGCATGTATTGAACAGCGACCTGAT) was used as a matrix to produce an initial array of 12 × 197 bp DNA repeats. An *Ava*I restriction site was introduced at the end of the 601 DNA sequence by PCR. *Ava*I-digested 601 Widom DNA fragments were ligated and the ligation reaction was loaded on an agarose gel. The band migrating at ∼2400 bp (corresponding to 12 repeats) was eluted from the gel and purified. The 12 × 197 bp 601 DNA array was then cloned into a pGEMT-easy plasmid (Promega). Left and right 6 × 197 bp (wild-type 601) DNA repeats were prepared in a similar way and subsequently ligated to each end of the central 12 × 197 bp DNA fragment. The resulting 24 × 197 bp wild-type array sequence was then cloned into the pGEMT vector. The linker and core DNA of each repeat contains an *Ava*I and *Hha*I restriction site, respectively.

Design and assembly of the central N1-N12 DNA fragment

12 different constructs (N1 to N12) were designed based on the Widom 601 147 bp sequence (Figures 3A and S5). Each construct contains a unique restriction site within the linker DNA, allowing for the specific replacement of a selected repeat by a biotin-labeled repeat. Each construct also contains a unique three-nucleotide barcode within the core 601 sequence on both the entry and exit sides, allowing for the specific amplification and detection of the core nucleosome DNA of interest. A *Sca*I restriction site within each repeat allows digestion of the array into individual mononucleosomes. The core DNA of each of the 12 repeats contains a *Hha*I restriction site. Unlike the carrier DNA, the central N1-N12 DNA fragment lacks an *Ava*I site. The assembly of the N1-N12 DNA fragment was achieved in a modular way starting from the construction of four tri-repeat fragments (N1-N3, N4-N6, N7-N9 and N10-N12). To construct the N1-N3 fragment, monomers N1, N2 and N3 were PCR amplified using the uniquely barcoded 601 DNAs as a template. N1 was digested with *Afl*II, N2 with *Afl*II and *Bam*HI, and N3 with *Bam*HI. The digested N2 fragment was dephosphorylated. These fragments were mixed in a 1:2:1 molar ratio and ligated overnight at 4°C. This scheme allows only the correct N1-N3 fragment to be assembled while other unwanted ligation products are eliminated. The ligation was checked on a 1.5% agarose gel. The N1-N3 trimer, hereafter called Trimer 1 (T1), was purified on agarose gel. Using the same strategies and conditions, N4-N6, N7-N9 and N10-N12 were purified and designated as Trimer 2 (T2), Trimer 3 (T3) and Trimer 4 (T4), respectively. T1 and T2 were digested by *Bst*b1 and ligated to form a tandem of six repeats (named S1), which was purified on agarose gel using the same conditions. T3 and T4 were digested by *Hin*dIII, ligated and purified in order to obtain the second tandem of six repeats (S2). pGEMT-easy vectors were modified to include within their multiple cloning site (MCS) restriction sites for *Eco*RI and *Bgl*II (for S1) and *Bgl*II and *Eco*RV (for S2). In turn, S1 was digested by *Eco*RI and *Bgl*II and S2 digested by *Bgl*II and *Eco*RV and each was separately cloned into the corresponding pGEMT-easy vector. After amplification of the constructs, the S1 and S2 inserts were isolated and ligated together, and the ligation products subsequently separated on an agarose gel. The desired band of 2400 bp (corresponding to the N1-N12 fragment) was excised from the gel and purified.

Assembly of the 24 × 197 bp (N1-N12) DNA

One 6 × 197 bp wild-type 601 DNA repeat was ligated to each end of the N1-N12 DNA fragment and the resulting 24 × 197 bp sequence was then cloned into the pGEMT vector. The vector was amplified and the 24 × 197 bp sequence was then purified after restriction enzyme cleavage of the vector.

Construction of 24 × 197 bp (N1-N12) DNA specifically biotinylated on repeat N4 or N5

Biotinylated N4 and N5 DNA fragments were generated by PCR amplification using biotinylated primers. The primer sequences used are shown below (**A** and **T** indicate biotinylated adenine and thymine, respectively; these positions correspond to nucleotides located outside the nucleosomal core DNA sequence):

Biotinylated repeat		Primer sequence
N4	Forward	5′ CATCAGTACTAGGTCTTCGAACA ATACATGC**A**CAGGATGTA 3′
	Reverse	5′ GTGCATGTATTGACATATGA CCTAGTACTGA**T**GGACCCTATACG 3′
N5	Forward	5′ CTAGGTCATATGTCAATACATGC**A**CAGGATG 3′
	Reverse	5′ TATTGAACGTGCACCTAGTACTGA **T**GGACCCTATACGC 3′

For the incorporation of the N4-biotin repeat, calf intestinal phosphatase (CIP)-treated 24 × 197 bp (N1-N12) DNA was digested by *Nde*I and *Bst*I and the resulting N1-N3 and N5-N12 fragments were purified. The PCR-produced N4-biotin (N4B) was digested by *Nde*I and then ligated with the N5-N12 fragment. The ligation product, corresponding to N4B-N12, was purified and subsequently digested with *Bst*BI. The digested N4B-N12 fragment was then ligated with the N1-N3 fragment and the resulting 24 x197 bp

(N1-N12) array containing biotinylated N4 was gel purified. The 24 × 197 bp (N1-N12) array containing biotinylated N5 was generated similarly, except that *Apa*LI and *Nde*I were used instead of *Nde*I and *Bst*BI, respectively.

Reconstitution of the 24-nucleosome array

Xenopus laevis histone mutants H4 V21C, H3 C111A, H2A E64C and the wild-type H2B were produced using a well established protocol (Roulland et al., 2016). The histone octamer was prepared using equimolar amounts of the different core histones. 24 × 197 bp (N1-N12) arrays and 24 × 197 bp (wild-type 601) carrier arrays (at ratio 1:25) were mixed in equimolar ratio with histone octamers in HFB buffer (2 M NaCl, 10 mM Tris-HCl pH 7.4, 1 mM EDTA and 100 mM DTT). The mixture was transferred into dialysis tubing and the reconstitution was performed by dialysis against a slowly decreasing salt buffer down to 500 mM NaCl with the help of a peristaltic pump. The dialysis bags were then transferred to 300 mM NaCl buffer (300 mM NaCl, 10 mM Tris-HCl pH 7.4, 0.25 mM EDTA, 10 mM β-mercaptoethanol) for 2 h, followed by a final dialysis overnight in 10 mM NaCl buffer (10mM NaCl, 10 mM Tris-HCl pH 7.4, 0.25 mM EDTA, 10 mM β-mercaptoethanol). Then NAP-1 mediated H1 deposition on nucleosome arrays was carried out. Briefly, full-length histone H1 was mixed with histone chaperone NAP1 at 1:2 molar ratio and incubated for 30 min at 30°C in the following buffer: 20 mM Tris-HCl pH 7.4, 0.5 mM EDTA, 100 mM NaCl, 1 mM DTT, 10% glycerol, 0.1 mM PMSF. Afterward the incubation mixture was added to the nucleosome arrays at a 1.25:1 ratio and incubated for 1 h at 30°C. The integrity of the nucleosome arrays was verified by digestion with *Ava*I/*Sca*I or *Hha*I restriction endonucleases.

Disulfide Crosslinking

Chromatin was first dialyzed against crosslinking buffer (10 mM Tris pH 9, 50 mM NaCl, 250 μM EDTA) for 3 h at room temperature using the cellusepT2 dialysis tubing 10 mm width. After dialysis, the chromatin (30 ng/μl) was adjusted to 25 μM of oxidized glutathione, 50 mM NaCl, 10 mM Tris pH 9 and was incubated at 37°C overnight for histone-histone crosslinking. Increasing the ionic strength to 80 mM NaCl during crosslinking yielded identical results as those observed at 50 mM NaCl.

Digestion and DTT treatment

Before *Sca*I/*Ava*I digestion, the crosslinked chromatin was incubated with 2.5 mM iodoacetamide at room temperature in the dark for 1 h. The mixture was subsequently dialyzed against NT buffer (50 mM NaCl, 10 mM Tris pH 7.4) for 5 h at 4°C. After dialysis, 5 μL of highly concentrated NapI (9.2 μg/μl) was added in order to remove the linker histone H1 from the chromatin. Chromatin was digested with 250 units of *Ava*I and 100 units of *Sca*I overnight at 37°C in 200 μL of buffer containing 10 mM Tris pH 7.4, 50 mM NaCl, 1.25 mM MgCl$_2$. The next day, each tube was separated in two volumes of 100 μL each. In one of these, 10 μL of 1 M DTT was added and in the other 10 μL of NT buffer. Reactions were incubated at room temperature for 2 h. The digestion and efficiency of DTT treatment were checked on a 1% agarose gel with 0.5X TBE before proceeding to affinity precipitation.

Chromatin Affinity precipitation (ChAP)

Each tube containing 2 μg of *Sca*I/*Ava*I-digested crosslinked chromatin (±DTT treatment) and 1.5 ng of internal control (IC) (random ~160 bp chicken erythrocyte DNA reconstituted nucleosomes or mononucleosomes reconstituted using the 5S *Xenopus* rDNA fragment) were incubated overnight at 4°C under 20 rpm shaking with 5 μl of BSA-blocked streptavidin magnetic beads (Dynabeads M-280 Streptavidin; Life Technology) in the presence of 0.05% NP40. The supernatant was discarded and beads were washed 3 times for 30 min with a buffer containing 10 mM Tris pH 7.4, 50 mM NaCl, 100 μM EDTA pH 8, 100 μg/ml BSA, 0.05% NP40 and 10 ng/μl erythrocyte chicken nucleosome. To recover the attached DNA, the beads, as well as 5% of the input ChAP reaction mixtures, were subjected to 1 μl of proteinase K treatment (934 U/ml; Fermentas) at 55°C for 2 h under rotation in 200 μl of STOP buffer (0.1% SDS, 20 mM EDTA). The supernatant was collected and DNA extracted by phenol/chloroform and precipitated by ethanol.

DNA quantification and qPCR

After DNA precipitation, 100 μL of TE was added to each tube and total DNA was quantified using the Quant-it Picogreen dsDNA assay kit (Invitrogen). 1 μL of each tube was deposited into wells of 96-well black plates (Corning), 200 μL of 1x Picogreen mix were added and incubated for 10 min before reading the fluorescence with Mithras LB 940 (multimode microplate reader; Berthold Technologies). The concentration of each sample (usually between 1.5 and 2 ng/μl) was determined with the help of a standard calibration curve. The DNA was diluted up to 16.6 pg/μl with ultrapure Millipore water and 3 μL (50 pg) were added to each well of qPCR 196-well plates (Eurogentec), together with 1x Sybr Green Mix (Fast start Universal SYBR Green; Roche) and 10 pmol/μl detection primers and completed to 15 μL with ultrapure water. The amplification was done on a StepOnePlus real-time PCR system (Applied Biosystem) and the enrichment was calculated. The calculated enrichments were normalized to the maximum signal corresponding to the respective biotinylated nucleosomal DNA. qPCR samples were run in triplicate. Usually, two independent experimental repeats were carried out for most experiments, showing a very high reproducibility with deviations of only a few percent.

Preparation of hexanucleosome array for crystal structure determination
Generation of 6 × 187 bp 601 DNA

The 6 × 187 bp 601 DNA sequence used for the reconstitution of the hexanucleosomes for crystallographic studies was constructed by a similar strategy as that for the 6 × 197 bp 601 DNA array described above. The final nucleotide sequence is as follows (core DNA is underlined):

5′ATCGCTGTTCAATACATGCA CAGGATGTATATATCTGACACGTGCCTGGAGACTAGGGAGTAATCCCCTTGGCGGTTAAAAC GCGGGGGACAGCGCGTACGTGCGTTTAAGCGGTGCTAGAGCTGTCTACGACCAATTGAGCGGCCTCGGCACCGGGATTCTC CAGGGCGGCCGCGTATAGGGTCTCGGGGCTGTTCAATACATGCA

CAGGATGTATATATCTGACACGTGCCTGGAGACTAGGGAGTAATCCCCTTGGCGGTTAAAACGCGGGGGACAGCGCGTACGT
GCGTTTAAGCGGTGCTAGAGCTGTCTACGACCAATTGAGCGGCCTCGGCACCGGGATTCTCCAGGGCGGCCGCGTATAGGG
TCTCGGGGCTGTTCAATACATGCA
CAGGATGTATATATCTGACACGTGCCTGGAGACTAGGGAGTAATCCCCTTGGCGGTTAAAACGCGGGGGACAGCGCGTACGT
GCGTTTAAGCGGTGCTAGAGCTGTCTACGACCAATTGAGCGGCCTCGGCACCGGGATTCTCCAGGGCGGCCGCGTATAGGG
TCTCGGGGCTGTTCAATACATGCA
CAGGATGTATATATCTGACACGTGCCTGGAGACTAGGGAGTAATCCCCTTGGCGGTTAAAACGCGGGGGACAGCGCGTACGT
GCGTTTAAGCGGTGCTAGAGCTGTCTACGACCAATTGAGCGGCCTCGGCACCGGGATTCTCCAGGGCGGCCGCGTATAGGG
TCTCGGGGCTGTTCAATACATGCA
CAGGATGTATATATCTGACACGTGCCTGGAGACTAGGGAGTAATCCCCTTGGCGGTTAAAACGCGGGGGACAGCGCGTACGT
GCGTTTAAGCGGTGCTAGAGCTGTCTACGACCAATTGAGCGGCCTCGGCACCGGGATTCTCCAGGGCGGCCGCGTATAGG
GTCTCGGGGCTGTTCAATACATGCA
CAGGATGTATATATCTGACACGTGCCTGGAGACTAGGGAGTAATCCCCTTGGCGGTTAAAACGCGGGGGACAGCGCGTACGT
GCGTTTAAGCGGTGCTAGAGCTGTCTACGACCAATTGAGCGGCCTCGGCACCGGGATTCTCCAGGGCGGCCGCGTATAGGG
TGAT

Reconstitution of hexanucleosome array

The 6 × 187 bp 601 nucleosomal array was reconstituted using purified-to-homogeneity human core histones by the salt gradient dialysis method, as described above for the 24 × 197 bp 601 DNA array. Full-length *Xenopus laevis* histone H1.0b was added to the hexanucleosome in an equimolar ratio relative to the core histone octamer at 0.6 M NaCl and the sample was further dialyzed in 10 mM NaCl, 0.25 mM EDTA, Tris-HCl pH 7.6. Sample quality was verified by native agarose and SDS-polyacrylamide gel electrophoresis (Figure 1A).

Hydroxyl-radical footprinting analysis of a hexanucleosome array

The pGEM-T plasmid harboring the N1-N12 sequence was digested with *Eco*RI and *Bgl*II. The resulting 6 × 197 bp DNA fragment spanning repeats N1-N6 was gel purified and subsequently radiolabeled with ^{32}P on the 3′ end by Klenow fill-in. Hydroxyl-radical footprinting was carried out in a 15 μl reaction mixture containing 150 ng of either H1-bound or unbound radiolabeled nucleosomes. The hydroxyl radicals were generated by mixing 2.5 μl each of 2 mM FeAmSO$_4$/4 mM EDTA, 0.1 M ascorbate, and 0.12% H$_2$O$_2$ together in a drop on the side of the reaction tube before mixing rapidly with the reaction solution. After digestion for 2 min with hydroxyl radicals (see Syed et al., 2010), the reaction was arrested by the addition of 100 μL stop solution (0.1% SDS, 25 mM EDTA, 1% glycerol, and 100 mM Tris, pH 7.4), and the DNA was purified by phenol/chloroform extraction and ethanol/glycogen precipitation. The denatured DNA samples were run on an 8% denaturing polyacrylamide gel in 1X TBE buffer. The gels were dried and exposed overnight and imaged on a phosphorimager (Fuji-FLA5100). Gel scans were analyzed by Multi-Gauge (Fuji) software.

Crystal structure determination and analysis
Crystallization

Crystals were grown using the hanging drop vapor diffusion method at 20°C by mixing equal volumes of the hexanucleosome-H1 complex (1.3 μM) and crystallization solution containing 15% MPD, 0.1 M NaCl and 0.1 M Tris pH 8.8. Crystals were transferred to a mixture of mother liquor supplemented with MPD and ethylene glycol to a final concentration of 20% and 30% (v/v) respectively, and flash-cooled in liquid nitrogen.

Crystal structure determination

Diffraction data were collected at ESRF beamline ID23-1 on a Pilatus 6M-F detector. Data collection and statistics are summarized in Table 1. Data were integrated with XDS (Kabsch, 2010) and scaled using AIMLESS (Evans, 2006). Crystals belong to space group P22$_1$2$_1$ with one hexanucleosome per asymmetric unit and an estimated solvent content of 62.5%. The six nucleosome cores of the array were positioned by molecular replacement using the *X. laevis* NCP-601 crystal structure (Vasudevan et al., 2010) (PDB: 3LZ0) as a search model in PHASER (McCoy et al., 2007). Rigid-body and grouped B-factor refinement in Phenix (Adams et al., 2010) of the six NCPs of the hexanucleosome using data at 9.7 Å resolution gave R$_{cryst}$ and R$_{free}$ values of 0.3009 and 0.3538, respectively. At this stage the density of the entry/exit DNA extending from the six NCP areas was visible and was built by successive rounds of model building using Coot (Emsley et al., 2010) and rigid-body refinement in Phenix. The linker DNA connecting the six nucleosomes was gradually built into density, and its geometry was regularized and group B factors refined in Phenix. The amino acids of the histones from the *Xenopus* NCP model that differed from human were substituted using Coot, keeping the same orientation and best rotamers. Restrained XYZ refinement was then performed to improve geometry using 3UT9 and 3LZ0 as reference models. The final hexanucleosome model yielded R$_{cryst}$ and R$_{free}$ values of 0.2618 and 0.2907, respectively. Calculation of the composite omit map shown in Figure 1B and Video S1 was performed in Phenix (Adams et al., 2010) by iteratively omitting regions accounting for 5% of the entire structure; the omitted regions were then assembled to generate a map unbiased by the atomic model (Terwilliger et al., 2008).

Determination of helical parameters

Helical parameters listed in Figure S1 were calculated as follows. The nucleosome pseudodyad axis (x-axis) was determined using the CCP4 program Lsqkab (Kabsch, 1976) by fitting one H2A:H2B:H3:H4 tetramer onto the dyad-related tetramer; the nucleosomal superhelical axis (z-axis) was calculated as in Tolstorukov et al. (2007); and the y-axis was given by the right-handed coordinate frame. The nucleosome center was defined as the point of intersection of the x- and z-axes. The polar rotation angle θ_i relating nucleosome N_i to N_{i+1} and the unit vector $\mathbf{v}_i$ along the corresponding rotation axis were determined using Lsqkab by fitting the core histones of nucleosome N_i onto those of N_{i+1}. The fiber axis was calculated as $<\mathbf{p}_i> + t<\mathbf{v}_i>$, where t is an arbitrary scalar, $\mathbf{p}_i$ is the midpoint between the centers of N_i and N_{i+1}, and $<\mathbf{p}_i>$ and $<\mathbf{v}_i>$ are the mean values of $\mathbf{p}_i$ and $\mathbf{v}_i$ over all nucleosomes in the array. The angular deviation between the individual $\mathbf{v}_i$ vectors and the fiber axis ranged from $1.7°$ to $8.8°$ (mean: $5.1° \pm 2.9°$). Parameters α_i, β_i and γ_i (the angles between the fiber axis and the x-, y- and z-axes of nucleosome N_i, respectively) were calculated as $\arccos(\mathbf{f} \cdot \mathbf{e}_i)$, where $\mathbf{f}$ and $\mathbf{e}_i$ are unit vectors along the fiber axis and the relevant x_i-, y_i- or z_i- axis, respectively. The radial distance (r_i) was measured from the fiber axis to the nucleosome center. The rise (h_i) is the distance between successive nucleosome centers measured along the fiber axis.

Cryo-electron microscopy

Nucleosomal arrays comprising 6 × 187 bp and 12 × 197 bp 601 sequence (prepared as described above for crystallization) were dialyzed overnight to obtain the final desired NaCl or $MgCl_2$ concentration mentioned in the text, and concentrated in the dialysis buffer to a final DNA concentration of ∼200 ng/μL. 3 μl of each sample were deposited on previously glow-discharged (25 mA, 30 s, 10^{-1} Pa) Quantifoil 1.2/1.3 grids and flash frozen in liquid ethane using an automated plunger (Vitrobot, FEI) with controlled blotting time (1 s), blotting force (1), wait time (0), humidity (100%) and temperature (4°C). Images were recorded on either a Tecnai Sphera F20 (FEI) microscope operating at 200 kV and equipped with a 4kx4k Ceta (FEI) camera or a Tecnai Sphera G20 (FEI) microscope operating at 120 kV and equipped with a GATAN Ultrascan 1000 camera. Images were recorded under low-dose conditions (< 20 e/A^2) with a nominal underfocus between 2 and 2.7 μm to enhance particle contrast. The pixel size of recorded images was 0.414 nm and 0.702 nm for the F20 and G20, respectively. Images shown in Figures 6, S6, and S7 were processed in Adobe Photoshop. For field images (Figure S6), particle contrast was enhanced by manually adjusting the brightness and contrast levels, followed by application of a Gaussian blur using a 1 pixel radius. The same processing was also performed for magnified particle images (Figures 6, S6, and S7) except that an initial high pass filter step (50 pixel radius) was included to remove the background gradient.

Small-angle scattering

Hexanucleosomes (prepared as described above for crystallization) were dialysed overnight against a buffer containing 5 mM Tris-HCl pH 7.5, 0.25 mM EDTA and either 1, 50 or 90 mM NaCl. (Excessive sample precipitation hampered measuring data at higher NaCl concentrations). The final sample concentrations used were 135, 100 and 80 μg/mL for samples in 1, 50 and 90 mM NaCl, respectively. SAXS data were collected at an X-ray energy of 8 keV at ESRF beamline BM29. Scattered X-rays were recorded on a Pilatus 1M detector (Dectris) at a distance of 2.879 m from the sample. Samples were automatically loaded into a vacuum-mounted quartz-capillary of 1.8 mm in diameter. 40 μL were loaded for each sample and 10 frames of 0.8 s duration were collected at 20°C. Samples were flowed constantly through the capillary during measurement to minimize the effect of radiation damage. Processing of individual frames, including azimuthal integration to obtain the one-dimensional scattering curve, was performed using a processing pipeline within the EDNA framework (Brennich et al., 2016). Primary data reduction was performed using the program PRIMUS (Konarev et al., 2003). Time frames were combined, excluding frames affected by aggregation due to radiation damage, to give the average scattering curve for each measurement. The average scattering from the buffer alone, measured before and after each sample, was used for background subtraction. Model-independent scattering parameters (R_g and D_{max}) were determined using PRIMUS. The Fourier transform was calculated using the program GNOM (Svergun, 1992). For each sample, program DAMMIN (Svergun, 1999) was used to calculate 15 *ab initio* models which were averaged and filtered using DAMAVER (Volkov and Svergun, 2003). The program CRYSOL (Svergun et al., 1995) was used to calculate the theoretical scattering from the 6-mer crystal structure, modified to include GH1 and histone tail residues so as to ensure that the molecular mass matched that of the sample. (GH1 was modeled in an on-dyad position; core and H1 histone tails were modeled in an arbitrary extended conformation using the NIH Bax group pdb utilities server https://spin.niddk.nih.gov/bax/nmrserver/pdbutil/ext.html).

Analytical ultracentrifugation

Hexanucleosomes (prepared as described above for crystallization) were dialyzed overnight against a buffer containing (i) 5 mM Tris-HCl pH 7.5, 0.25 mM EDTA and either 1 or 90 mM NaCl or (ii) 5 mM Tris-HCl pH 7.5 and either 0.35, 0.5 or 0.6 mM $MgCl_2$. Hexanucleosome concentrations ranged from 14 to 28 μg/mL. Sedimentation velocity experiments were performed on a Beckman XL-I analytical ultracentrifuge equipped with an AN-50 TI rotor (Beckman Instruments) at 20°C, using 450 μL samples loaded into two-channel 1.2 cm path-length centerpieces with Sapphire windows (Nanolytics). Absorbance at 260 nm was measured in continuous scan mode during sedimentation at 18,000 rpm. Data were processed with Redate software (v. 1.0.1) and analyzed in terms of $c(s)$ distributions using SEDFIT (v. 14.1) and Gussi (1.2.1). $s_{20,W}$ values (sedimentation coefficient corrected for water at 20°C) were calculated with a partial specific volume of 0.622 ml/g for chromatin and solvent density and viscosity calculated using SEDNTERP. The $c(s_{20w})$ distributions were then converted into percent boundary fractions and the average sedimentation coefficients (s_{ave}) were determined at the boundary midpoint. The frictional ratio f/f_0 was derived from s_{ave} in the Svedberg equation. We observed a small

amount (< 13%) of dissociation of the hexanucleosome in 90 mM NaCl (as revealed by the presence of free DNA sedimenting at $s_{20,w}$ = 9S), reminiscent of the behavior of oligonucleosomes in the absence of H1 under similar ionic conditions (Hansen et al., 1989); dissociation was negligible in all other ionic conditions tested. Predicted sedimentation coefficients were calculated from the 6-mer crystal structure (modified to include H1 and histone tails as described above for SAXS analysis) and twisted 6-mer model (based on nucleosomes N1-N6 of Song et al., 2014, and modified to include histone tails as described above) using the Zeno method in program Ultrascan SOMO (Revision 3087).

QUANTIFICATION AND STATISTICAL ANALYSIS

ICNN and hydroxyl radical footprinting experiments were each performed at least twice. The qPCR samples were run in triplicate. The hydroxyl radical footprinting experiment was performed six times under slightly different experimental and gel conditions, each time yielding identical results. The highest quality gel images are presented in Figure 7B.

DATA AND SOFTWARE AVAILABILITY

The crystallographic model coordinates have been deposited in the Protein Data Bank under accession code 6HKT. SAXS data and data from ICNN experiments and hydroxyl radical footprinting have been deposited in the Mendeley Data repository: https://doi.org/10.17632/348t5n4m6k.1

Supplemental Information

Structure of an H1-Bound 6-Nucleosome

Array Reveals an Untwisted Two-Start

Chromatin Fiber Conformation

Isabel Garcia-Saez, Hervé Menoni, Ramachandran Boopathi, Manu S. Shukla, Lama Soueidan, Marjolaine Noirclerc-Savoye, Aline Le Roy, Dimitrios A. Skoufias, Jan Bednar, Ali Hamiche, Dimitar Angelov, Carlo Petosa, and Stefan Dimitrov
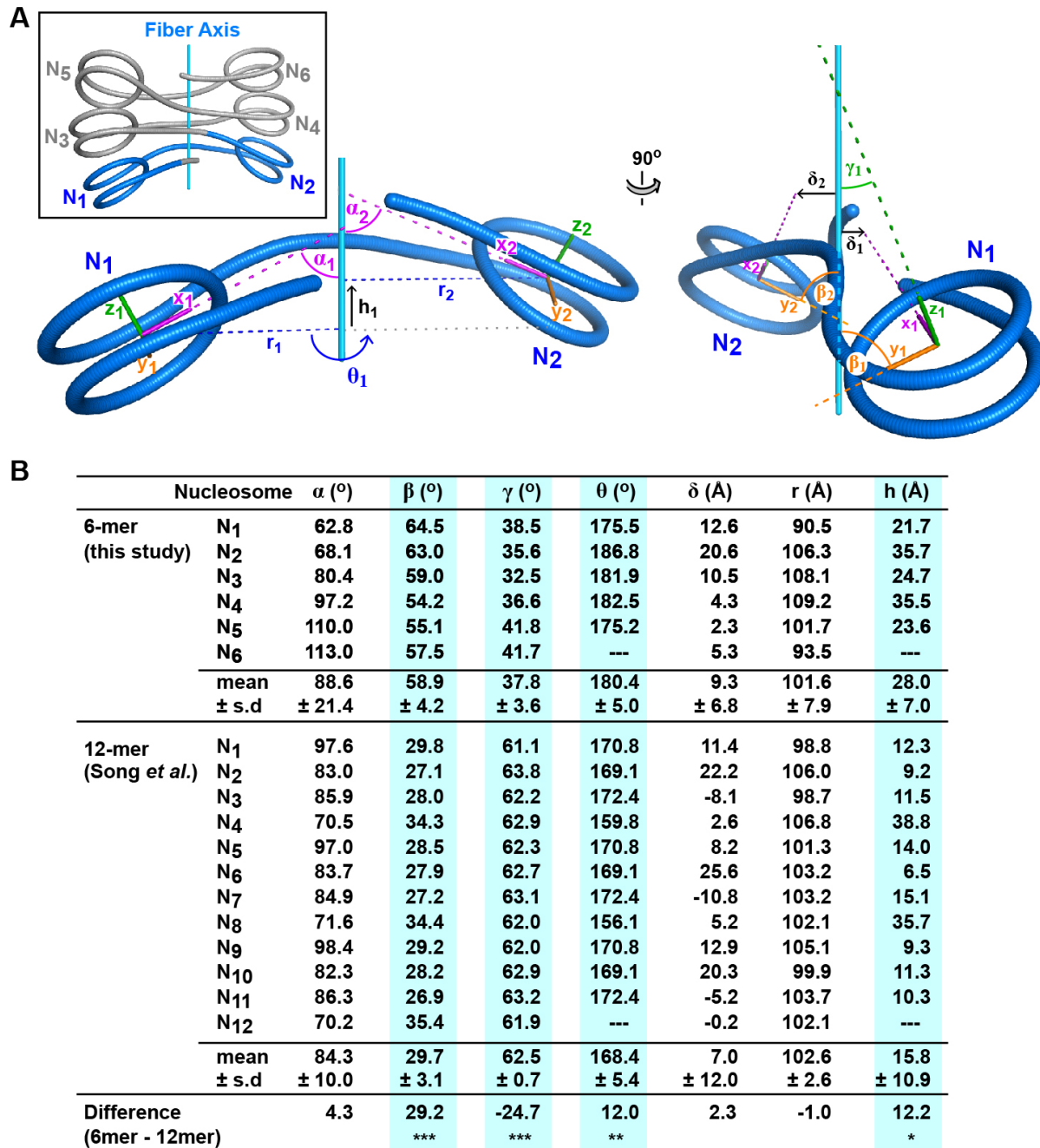
A.

B.

	Nucleosome	α (°)	β (°)	γ (°)	θ (°)	δ (Å)	r (Å)	h (Å)
6-mer	N_1	62.8	64.5	38.5	175.5	12.6	90.5	21.7
(this study)	N_2	68.1	63.0	35.6	186.8	20.6	106.3	35.7
	N_3	80.4	59.0	32.5	181.9	10.5	108.1	24.7
	N_4	97.2	54.2	36.6	182.5	4.3	109.2	35.5
	N_5	110.0	55.1	41.8	175.2	2.3	101.7	23.6
	N_6	113.0	57.5	41.7	---	5.3	93.5	---
	mean	88.6	58.9	37.8	180.4	9.3	101.6	28.0
	± s.d	± 21.4	± 4.2	± 3.6	± 5.0	± 6.8	± 7.9	± 7.0
12-mer	N_1	97.6	29.8	61.1	170.8	11.4	98.8	12.3
(Song *et al.*)	N_2	83.0	27.1	63.8	169.1	22.2	106.0	9.2
	N_3	85.9	28.0	62.2	172.4	-8.1	98.7	11.5
	N_4	70.5	34.3	62.9	159.8	2.6	106.8	38.8
	N_5	97.0	28.5	62.3	170.8	8.2	101.3	14.0
	N_6	83.7	27.9	62.7	169.1	25.6	103.2	6.5
	N_7	84.9	27.2	63.1	172.4	-10.8	103.2	15.1
	N_8	71.6	34.4	62.0	156.1	5.2	102.1	35.7
	N_9	98.4	29.2	62.0	170.8	12.9	105.1	9.3
	N_{10}	82.3	28.2	62.9	169.1	20.3	99.9	11.3
	N_{11}	86.3	26.9	63.2	172.4	-5.2	103.7	10.3
	N_{12}	70.2	35.4	61.9	---	-0.2	102.1	---
	mean	84.3	29.7	62.5	168.4	7.0	102.6	15.8
	± s.d	± 10.0	± 3.1	± 0.7	± 5.4	± 12.0	± 2.6	± 10.9
Difference (6mer - 12mer)		4.3	29.2 ***	-24.7 ***	12.0 **	2.3	-1.0	12.2 *

Figure S1. Related to Figure 1. Fiber parameters of the nucleosomal array. A. Definition of parameters. Each nucleosome is associated with a right-handed coordinate frame in which the *x*-axis represents the nucleosome pseudodyad axis, the *z*-axis represents the superhelical axis, and the *y*-axis lies in the plane of the nucleosomal disc. The parameter θ_i is the polar (azimuthal) rotation angle relating nucleosome N_i to N_{i+1}. Parameters α_i, β_i and γ_i are the angles between the fiber axis and the *x*-, *y*- and *z*-axes of nucleosome N_i, respectively. The radial distance (r_i) is measured from the fiber axis to the nucleosome center. The rise (h_i) is the distance between successive nucleosome centers measured along the fiber axis. The nucleosomal pseudodyad does not intersect the fiber axis but exhibits a slight offset, δ_i, defined as the perpendicular distance from the fiber axis to the pseudodyad. (See Methods for details of parameter determinations). **B.** Table of fiber parameters for the hexanucleosomal array and for the condensed 12-mer (Song et al., 2014). Parameters which differ significantly between the two arrays (as determined by a one-sided Mann-Whitney *U* test) are highlighted in cyan (***, $p<0.001$; **, $p<0.01$; *, $p<0.05$).
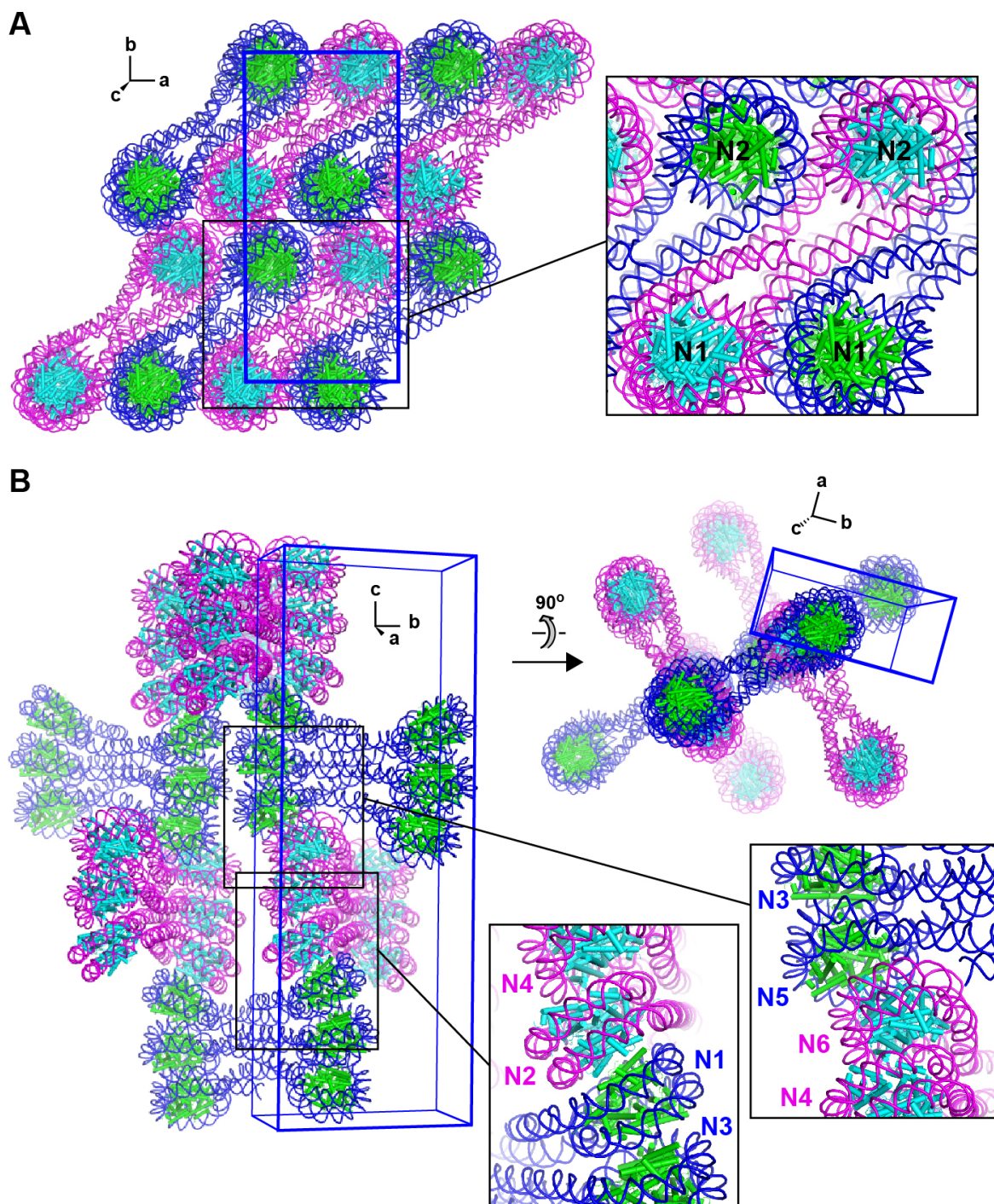
Figure S2. Related to Figure 1. Crystal packing interactions. Hexanucleosomes pack side-by-side in horizontal layers like mosaic tiles. Vertical stacking interactions between layers are mediated by the peripheral nucleosomes. **A.** View along the crystallographic *c*-axis showing one layer of hexanucleosomes in the *a-b* plane. The unit cell is shown in blue. The nucleosome cores of one array interact edge-to-edge with those of its neighbors. All the hexanucleosomes shown have the same polarity. **B.** View of vertical stacking interactions. For clarity, only a subset of molecules in the unit cell are shown. The two 3-nucleosome stacks of each hexanucleosome form a continuous column with the 3-nucleosome stacks from neighboring hexanucleosomes which are rotated by 90° along the fiber axis (*c*-axis) direction. The different nucleosome tilt angles (angle α in **Figure S1**) allow nucleosomes N1 and N5 to stack against nucleosomes N2 and N6 from neighboring arrays.
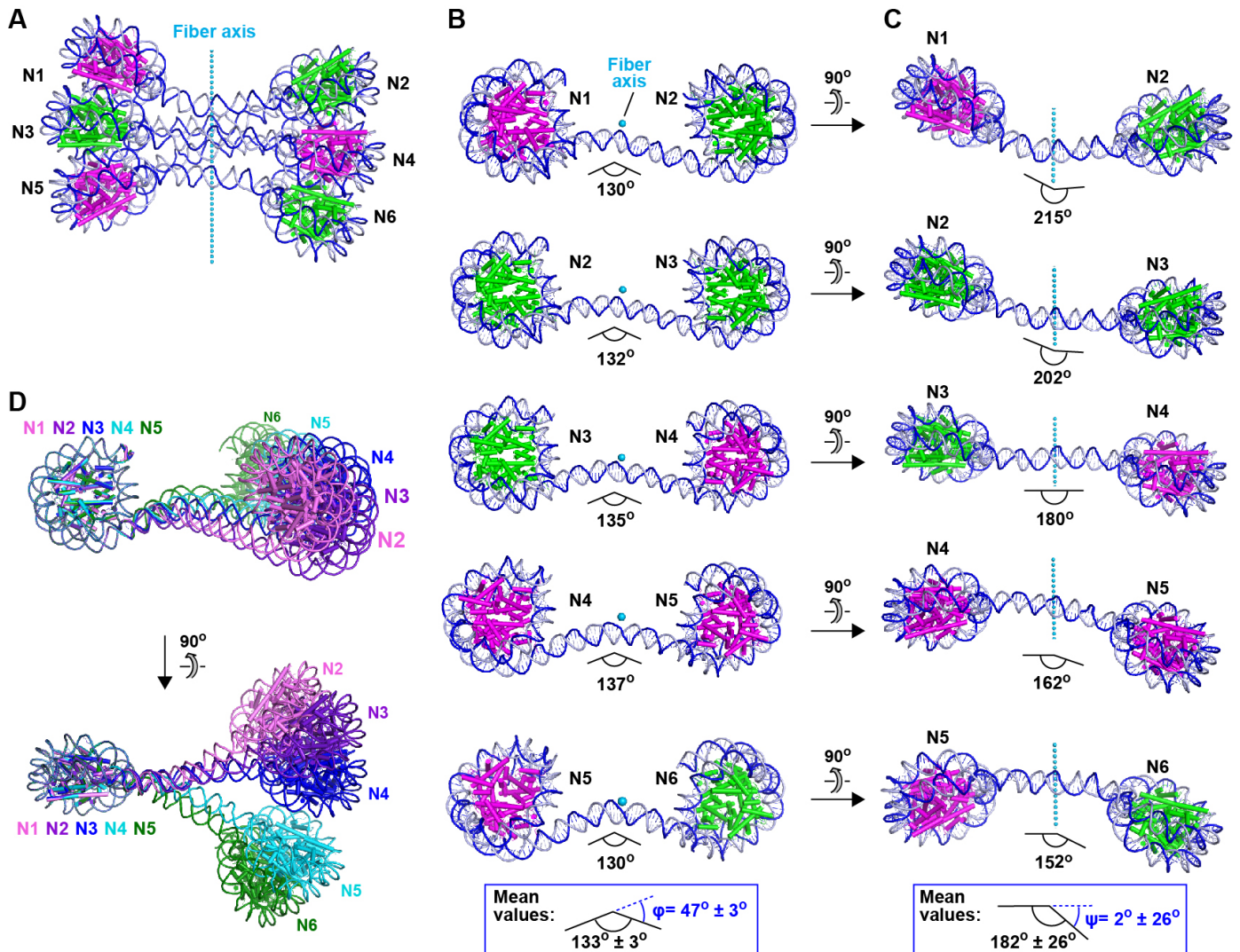
Figure S3. Related to Figure 1. Bending of the linker DNA. A. Global view of the 6-nucleosome array showing the direction of the fiber axis. **B.** Axial view of dinucleosome units showing the DNA bending angle in the plane orthogonal to the fiber axis. **C.** Side view showing the DNA bending angle in the plane of the fiber axis. **D.** Structural overlay of the first nucleosome in each dinucleosome unit showing the variation in linker DNA trajectory.
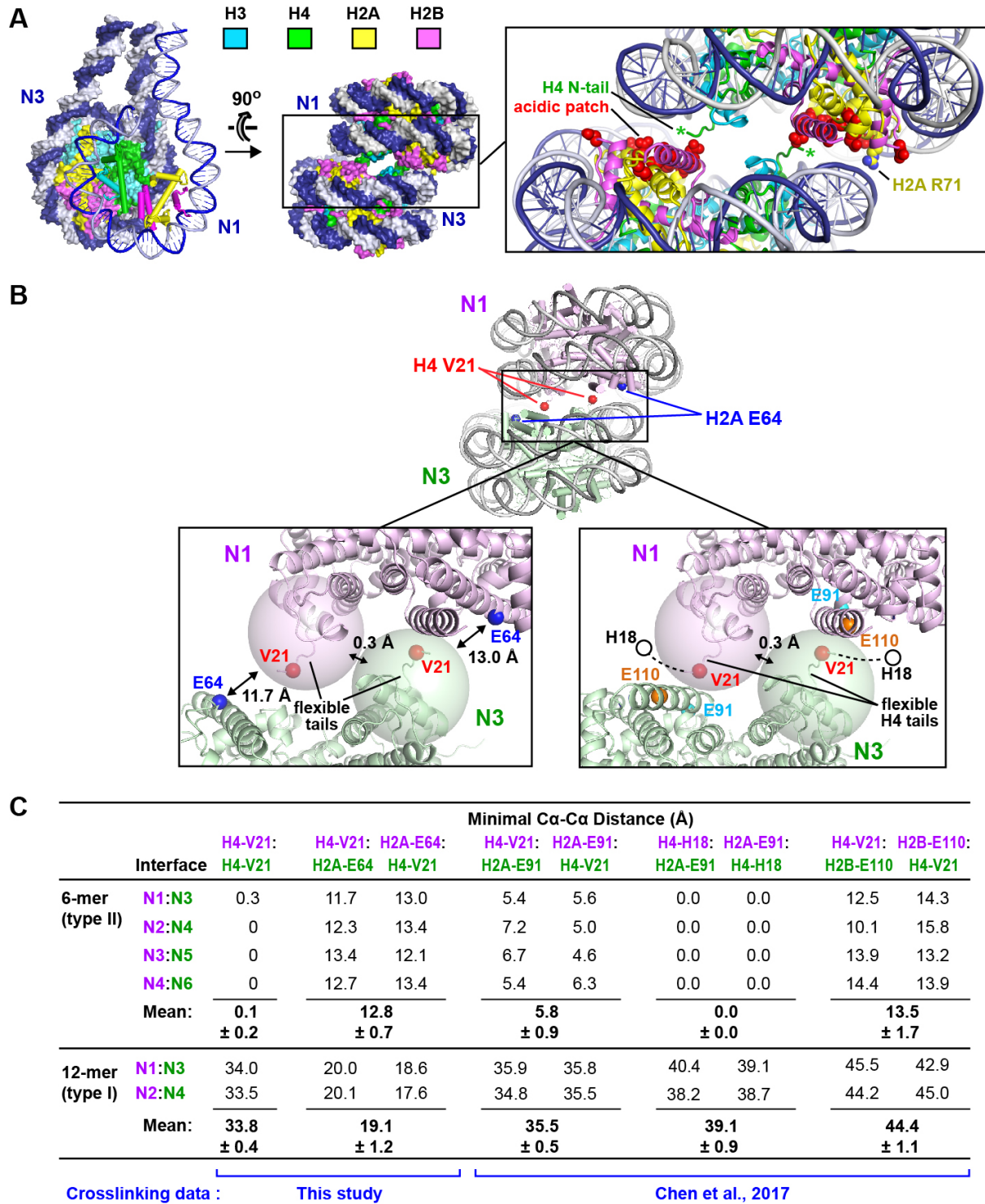
Figure S4. Related to Figure 3. The nucleosome stacking interface. A. Interactions in the N1:N3 interface. The location of flexible N-terminal H4 tail residues [16]KRHRKVLR[23] is indicated by a green asterisk. H2A-H2B acidic patch residues are shown as red spheres. For clarity, only half of nucleosome N1 is shown in the top left panel. H2A residue Arg71 is within contact distance of the DNA from the adjacent nucleosome; a minor change in nucleosome orientation would also allow H2B residues Lys105, His106, Lys113 and Lys117 to form such contacts. **B.** Compatibility of the 6-mer nucleosome stacking interface with disulfide crosslinking experiments. Besides the

crosslinks described in the text concerning Cys mutants introduced at positions H4 V21 and H2A E64, Chen *et al.* have recently reported internucleosomal disulfide bond formation between H4 V21C and either H2A E91C or H2B E110C, and between H4 H18 and H2A E91C (Chen et al., 2017). ***Left inset***, Location of H4 Val21 and H2A Glu64 in the N1:N3 interface. H4 residues 21-24 are within the flexible tail; the pink and green spheres indicate the maximal distance that H4 Val21 can be located from the first (non-flexible) residue in the H4 globular domain (Asn25). The minimal internucleosomal $C\alpha$-$C\alpha$ distance between mutated residues is indicated. (Histone tail positions shown are taken from PDB 3LZ0). ***Right inset***, Location of residues used for disulfide crosslinking experiments by Chen et al., 2017. The approximate location of H4 residue H18 is shown by an open black circle. **C.** Summary of minimal $C\alpha$-$C\alpha$ distances for pairs of residues located on opposite sides of each internucleosomal interface. The maximal $C\alpha$-$C\alpha$ distance between two disulfide-bonded residues is ~7 Å (Petersen et al., 1999). The observed $C\alpha$-$C\alpha$ distances are compatible with an internucleosomal disulfide bond between two H4 V21C residues. Disulfide formation between H4 V21C and H2A E64C would require only a small relative movement (5-6 Å) of adjacent nucleosomes. The size of the required movement is only twice the mean atomic displacement of our structure (2.6 Å; derived from the mean B-factor) and is feasible considering the loose nature of the interface. By the same token, the distances between residues implicated in the study by Chen et al., are all feasibly compatible with crosslink formation. By contrast, the corresponding distances in a type I interface are too large to permit disulfide crosslinks.
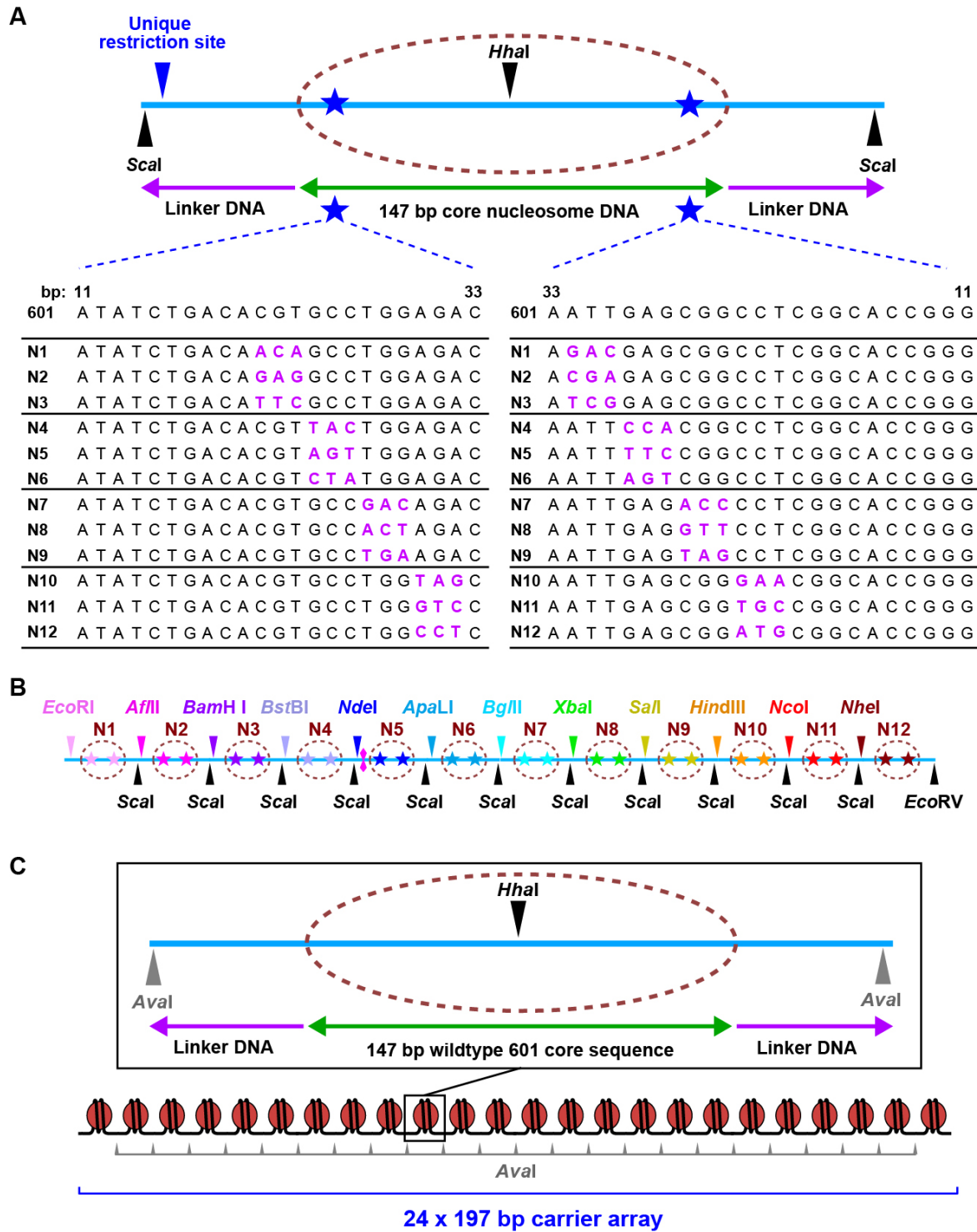
Figure S5. Related to Figure 3. Details of nucleosome arrays used for ICNN analysis. A,B. Unique features within the central N1-N12 DNA fragment. **A.** Summary of mutated nucleotides (in magenta) within the nucleosome cores of the N1-N12 fragment. **B.** Restriction sites present within the N1-N12 fragment. *Sca*I and *Eco*RV cleave DNA to yield blunt ends, *Nde*I and *Bst*BI leave a 5' overhang of 2 bp, and the remaining enzymes (*Eco*RI, *Afl*II, *Bam*H1, *Bst*BI, *Apa*LI, *Bgl*II, *Xba*I, *Sal*I, *Hin*dIII, *Nco*I and *Nhe*I) leave a 5' overhang of 4 bp. **C.** Schematic representation of the 24-nucleosome carrier array. Note the absence of the unique nucleotides and restriction sites shown in panels **A** and **B**. A 25-fold excess of carrier DNA was used to suppress qPCR signals arising from non-specific cross-linking between nucleosome arrays (interfiber crosslinks).
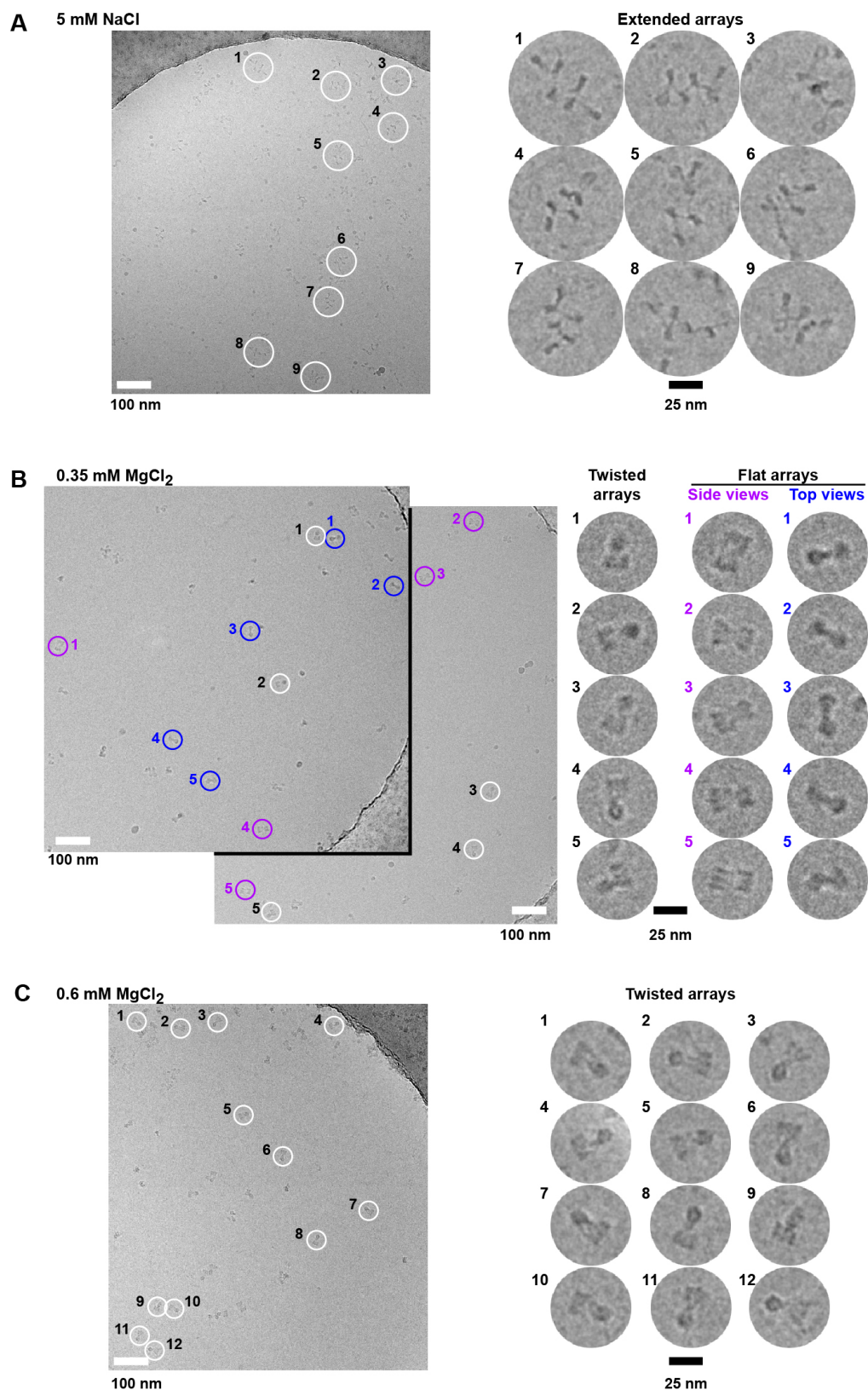
Figure S6. Related to Figure 6. Cryo-EM images of 6-nucleosome arrays in the presence of monovalent or divalent cations. A-C. Images of 6 x 187 bp nucleosome arrays dialyzed against (**A**) 5 mM NaCl, (**B**) 0.35 mM MgCl$_2$, and (**C**) 0.6 mM MgCl$_2$. *Left,* Micrographs showing a field of particles. Representative particles presenting characteristic views are circled. *Right,* Magnified views of particles circled in micrographs.
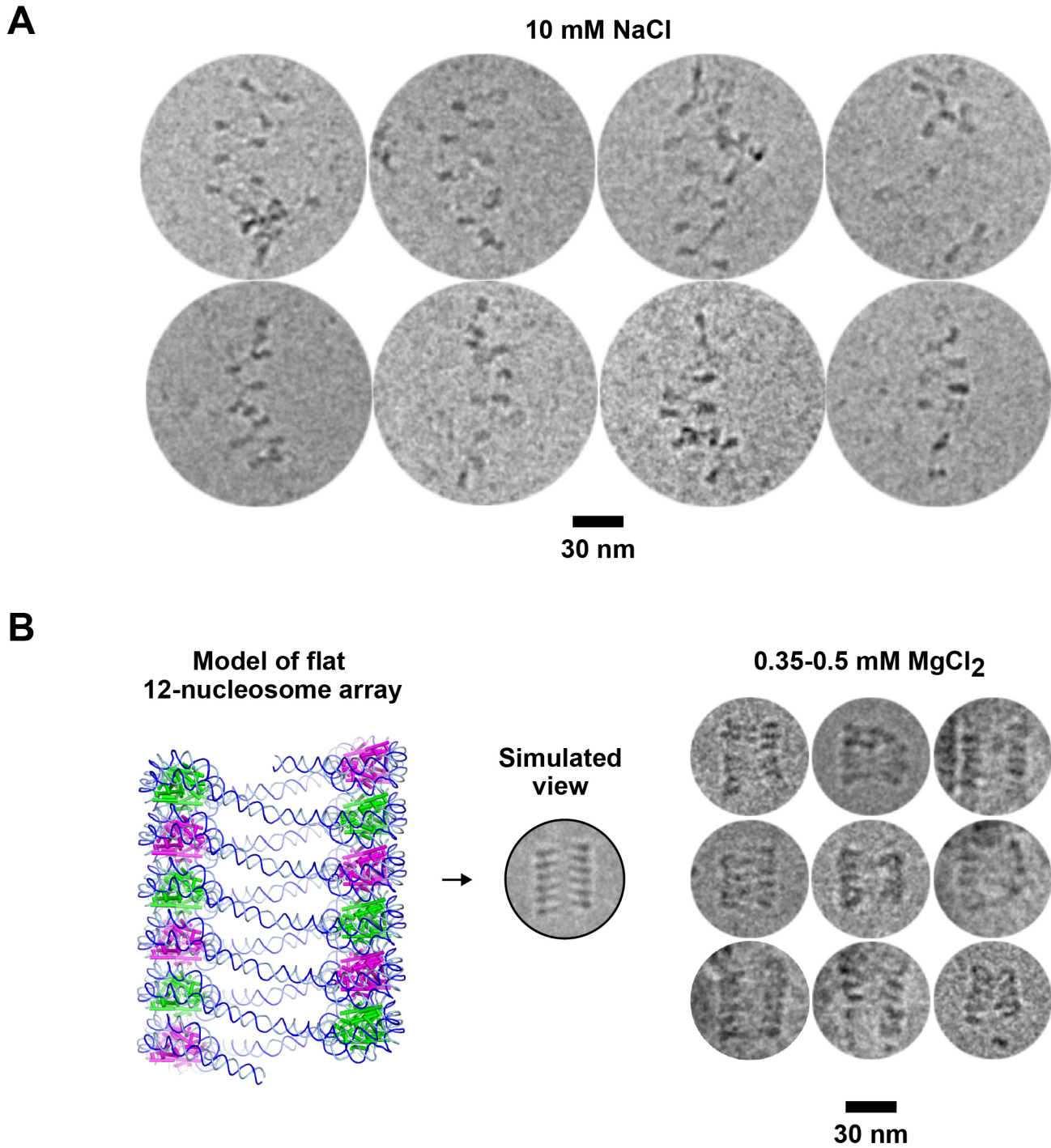
A

10 mM NaCl

30 nm

B

**Model of flat
12-nucleosome array**

0.35-0.5 mM MgCl$_2$

**Simulated
view**

30 nm

Figure S7. Related to Figure 6. Cryo-EM analysis of 12 x 197 bp nucleosome arrays. A. Particles in an open zigzag conformation in 10 mM NaCl. **B.** Particles in 0.35 – 0.5 mM MgCl$_2$ showing a ladder-like conformation. The view simulated from the model of an untwisted 12-nucleosome array derived from the 6-mer crystal structure (**Fig. 2**) is shown at the same scale for comparison.
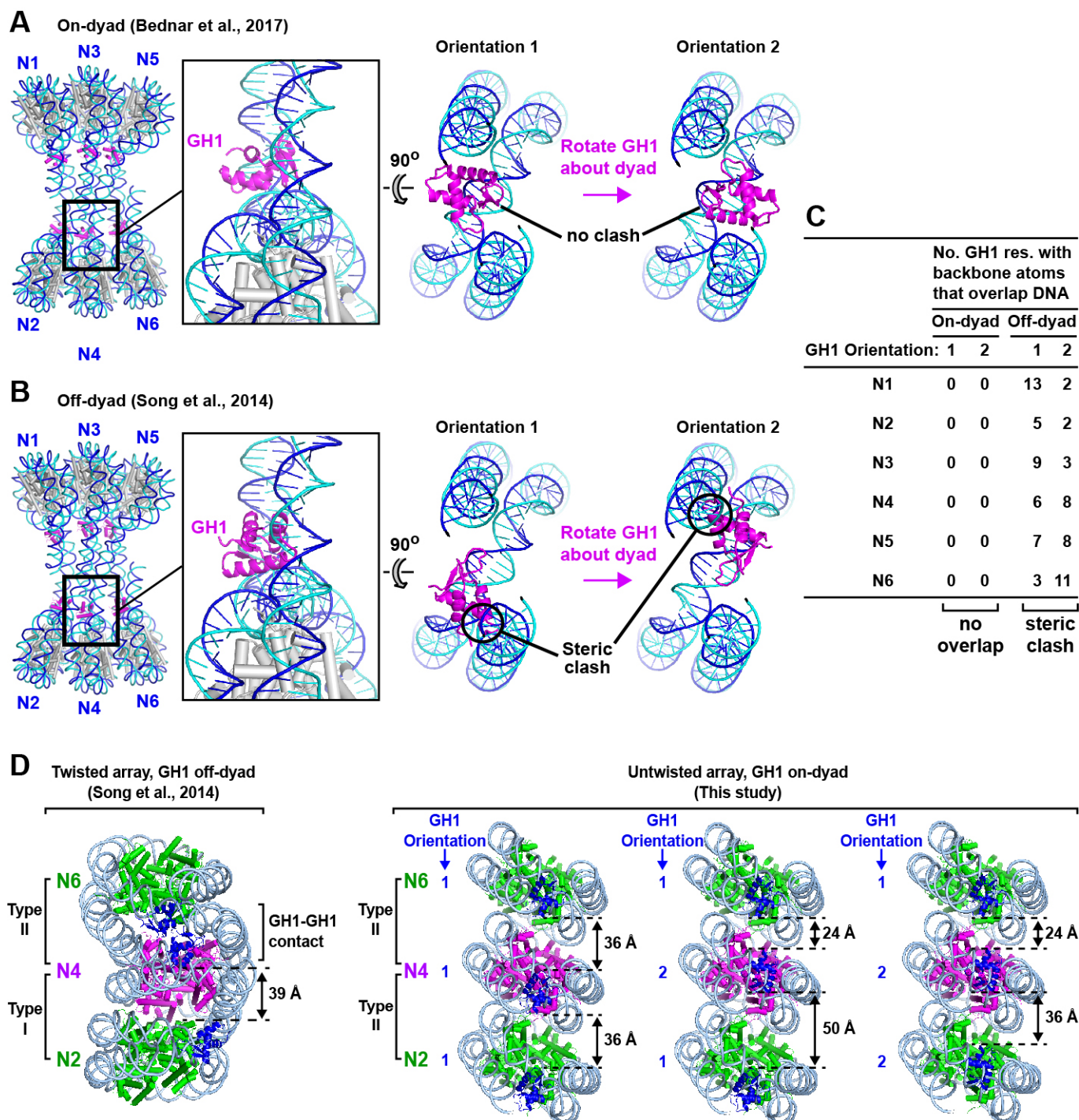
Figure S8. Related to Figure 7. Comparison of on- and off-dyad GH1 binding configurations. A. The on-dyad GH1 configuration observed in PDB 5NL0 (Bednar et al., 2017) was superimposed onto nucleosome N4 of the 6-mer crystal structure in both possible dyad-related orientations. No steric clashes involving the modeled GH1 and the hexanucleosomal DNA were observed in either orientation. **B.** The off-dyad GH1 configuration observed in the condensed 12-mer structure (Song et al., 2014) was superimposed onto nucleosome N4 of the 6-mer. In both dyad-related orientations the domain shows a severe steric overlap with the linker DNA of the 6-mer. **C.** Summary of steric clashes when on- and off-dyad GH1 configurations are superimposed onto each nucleosome within the 6-mer. The

number of GH1 residues with one or more main chain atoms less than 2 Å from a DNA atom is listed. **D.** GH1-GH1 interactions in twisted and untwisted arrays. GH1 domains are shown in blue. *Left*, GH1 domain interactions in the condensed 12-mer. GH1 domains on either side of a type I interface (within a tetranucleosome unit) are far apart, but those spanning a type II interface (between tetranucleosome units) are in close contact (Song et al., 2014). *Right*, Lack of GH1 domain interactions in an untwisted array. The GH1 domains were positioned on our model of an extended nucleosome array (**Figure 2B**) in an on-dyad configuration in the two possible dyad-related orientations. Neighboring GH1 domains are far apart regardless of the orientation adopted. Distances shown are those between the closest pair of Cα atoms on neighboring GH1 domains.